





ORIGINAL RESEARCH

# Phosphorus Supplementation Mitigates Perivascular Adipose Inflammation–Induced Cardiovascular Consequences in Early Metabolic Impairment

Haneen S. Dwaib , MSc\*; Ghina Ajouz, MSc\*; Ibrahim AlZaim , BPharm; Rim Rafah, MD, MSc; Ali Mroueh, MSc; Nahed Mougharbil, BS; Marie-Elizabeth Ragi , MSc; Marwan Refaat, MD; Omar Obeid, PhD; Ahmed F. El-Yazbi , PhD

**BACKGROUND:** The complexity of the interaction between metabolic dysfunction and cardiovascular complications has long been recognized to extend beyond simple perturbations of blood glucose levels. Yet, structured interventions targeting the root pathologies are not forthcoming. Growing evidence implicates the inflammatory changes occurring in perivascular adipose tissue (PVAT) as early instigators of cardiovascular deterioration.

**METHODS AND RESULTS:** We used a nonobese prediabetic rat model with localized PVAT inflammation induced by hypercaloric diet feeding, which dilutes inorganic phosphorus (Pi) to energy ratio by 50%, to investigate whether Pi supplementation ameliorates the early metabolic impairment. A 12-week Pi supplementation at concentrations equivalent to and twice as much as that in the control diet was performed. The localized PVAT inflammation was reversed in a dose-dependent manner. The increased expression of UCP1 (uncoupling protein1), HIF-1 $\alpha$  (hypoxia inducible factor-1 $\alpha$ ), and IL-1 $\beta$  (interleukin-1 $\beta$ ), representing the hallmark of PVAT inflammation in this rat model, were reversed, with normalization of PVAT macrophage polarization. Pi supplementation restored the metabolic efficiency consistent with its putative role as an UCP1 inhibitor. Alongside, parasympathetic autonomic and cerebrovascular dysfunction function observed in the prediabetic model was reversed, together with the mitigation of multiple molecular and histological cardiovascular damage markers. Significantly, a Pi-deficient control diet neither induced PVAT inflammation nor cardiovascular dysfunction, whereas Pi reinstatement in the diet after a 10-week exposure to a hypercaloric low-Pi diet ameliorated the dysfunction.

**CONCLUSIONS:** Our present results propose Pi supplementation as a simple intervention to reverse PVAT inflammation and its early cardiovascular consequences, possibly through the interference with hypercaloric-induced increase in UCP1 expression/activity.

**Key Words:** inorganic phosphorous ■ perivascular adipose inflammation ■ prediabetes ■ uncoupling protein 1

The past few decades have seen a staggering rise in global incidence of metabolic disorders including obesity<sup>1,2</sup> and type 2 diabetes.<sup>3</sup> Such an increase was associated with a growing health

and economic burden because of the escalating risk of mortality and morbidity attributable to cardiometabolic complications including ischemic heart disease, ischemic stroke, cardiac metabolic dysfunction, and

Correspondence to: Ahmed El-Yazbi, Department of Pharmacology and Toxicology, Faculty of Medicine, American University of Beirut, PO Box 11-0236, Riad El-Solh 1107 2020, Beirut, Lebanon. E-mail: Ahmed.fawzy.aly@alexu.edu.eg and Omar Obeid, Department of Nutrition and Food Science, Faculty of Agriculture and Food Sciences, American University of Beirut, PO Box 11-0236, Riad El-Solh 1107 2020, Beirut, Lebanon. E-mail: oo01@aub.edu.lb

\*H. S. Dwaib and G. Ajouz contributed equally.

Supplemental Material for this article is available at <https://www.ahajournals.org/doi/suppl/10.1161/JAHA.121.023227>

For Sources of Funding and Disclosures, see page 18.

© 2021 The Authors. Published on behalf of the American Heart Association, Inc., by Wiley. This is an open access article under the terms of the Creative Commons Attribution-NonCommercial-NoDerivs License, which permits use and distribution in any medium, provided the original work is properly cited, the use is non-commercial and no modifications or adaptations are made.

JAHA is available at: [www.ahajournals.org/journal/jaha](http://www.ahajournals.org/journal/jaha)

## CLINICAL PERSPECTIVE

### What Is New?

- Perivascular adipose tissue inflammation represents the initial response to metabolic challenge and leads to cardiovascular dysfunction early in the course of metabolic impairment.

### What Are the Clinical Implications?

- Increased UCP1 (uncoupling protein 1) expression and consequent increase in oxygen consumption might underlie the exaggerated hypoxia in perivascular adipose tissue and hence its increased vulnerability to inflammation compared with other adipose depots.
- Inorganic phosphorus supplementation inhibits UCP1 activity and offers an innovative approach to curb early cardiovascular deterioration in metabolic disease.

## Nonstandard Abbreviations and Acronyms

<b>AIN</b>	American Institute of Nutrition
<b>BAT</b>	brown adipose tissue
<b>CaSR</b>	calcium sensing receptor
<b>DMEM-LG</b>	Dulbecco's Modified Eagle's Medium-low glucose
<b>FGF23</b>	fibroblast growth factor-23
<b>HIF-1<math>\alpha</math></b>	hypoxia-inducible factor-1 $\alpha$
<b>HR</b>	heart rate
<b>IL-1<math>\beta</math></b>	interleukin-1 $\beta$
<b>Pi</b>	inorganic phosphate
<b>PTH</b>	parathyroid hormone
<b>PVAT</b>	perivascular adipose tissue
<b>UCP1</b>	uncoupling protein 1
<b>WAT</b>	white adipose tissue

heart failure.<sup>4,5</sup> At their root, these changes could be attributed to parallel shifts in lifestyle and dietary habits with increased consumption of refined, calorie-dense diets rich in saturated fats and simple sugars.<sup>6,7</sup>

Evidence accumulating over the past 2 decades implicated adipose tissue inflammation in response to chronic excessive caloric intake in the development of obesity and type 2 diabetes.<sup>8</sup> Several types of immune cells and inflammatory cytokines contribute to the adipose tissue inflammatory phenotype in this context.<sup>9,10</sup> Significantly, a long-standing association has been described between increased cardiovascular risk in the early stage of metabolic dysfunction including prediabetes and inflammatory changes,<sup>11</sup> with the latter potentially starting adipose tissue in response to insulin

resistance and hyperinsulinemia.<sup>12</sup> Specifically, recent studies showed that localized inflammation in select visceral adipose depots, mainly perivascular adipose tissue (PVAT), epicardial, and perirenal adipose tissue, contribute to the detrimental cardiovascular alterations early in the course of metabolic disease in the absence of disseminated adipose inflammation or gross metabolic dysfunction.<sup>13–18</sup>

In this regard, our laboratory has shown that PVAT demonstrated a higher sensitivity to inflammatory changes triggered by a mild hypercaloric challenge compared with other visceral adipose depots.<sup>13,14</sup> This was explained based on the unique nature of PVAT harboring the properties of both white and brown adipose tissue (WAT and BAT, respectively).<sup>19,20</sup> Whereas adipocytes in PVAT, like those in WAT, undergo hypertrophy in response to increased caloric intake, an increased expression of the BAT marker, UCP1 (uncoupling protein 1), is only seen in PVAT under such circumstances.<sup>14</sup> In BAT, UCP1 increases mitochondrial energy dissipation as heat during nonshivering thermogenesis, and its expression level is associated with increased oxygen consumption.<sup>21–23</sup> The localized concurrence of these events renders PVAT more vulnerable to hypoxia, and thus inflammatory changes. Multiple lines of evidence suggested that reducing PVAT inflammation led to improving cardiovascular impairment associated with metabolic disease. Various interventions were put forward comprising nonpharmacological approaches such as calorie restrictions and intermittent fasting,<sup>24</sup> as well as pharmacological tools ranging from antidiabetic drugs with anti-inflammatory properties to statins and mineralocorticoid receptor antagonists.<sup>14,17</sup> However, no tailored interventions have been forthcoming. Nevertheless, increased UCP1 expression was consistently shown to occur in PVAT and perirenal adipose in a nonobese prediabetic rat model in conjunction with inflammation and cardiovascular dysfunction,<sup>14,18</sup> raising the possibility of targeting UCP1 as a potential selective approach to reduce the negative consequences of PVAT inflammation.

Of great relevance, recent *in vitro* investigation identified inorganic phosphorus (Pi) as an inhibitor of UCP1.<sup>25</sup> Importantly, the shift to refined diets is almost always associated with a reduction in micronutrient intake encompassing minerals including Pi.<sup>26</sup> Moreover, low serum Pi levels are known to be associated with metabolic syndrome and increased risk of cardiovascular disease.<sup>27</sup> Previous studies from our laboratory showed that Pi supplementation in humans ameliorated the biochemical parameters associated with increased risk of metabolic syndrome and cardiovascular disease, such as postprandial lipemia,<sup>28</sup> postprandial blood glucose, and insulin concentration, as well as insulin sensitivity,<sup>29</sup> in

addition to improvement of energy metabolism in patients who are obese and overweight.<sup>30</sup> However, increased dietary intake of Pi was also implicated in the development of cardiovascular disorders,<sup>31</sup> possibly in a biphasic relationship whereby both low and high serum Pi levels are associated with increased cardiovascular risk.<sup>27</sup> Nevertheless, hypercaloric diets used in our previous studies to induce early PVAT inflammation diluted Pi to energy ratio by  $\approx 50\%$ . As such, we hypothesize that Pi supplementation of Western diets will likely reduce the early cardiovascular consequences of hypercaloric intake potentially by attenuating UCP1-triggered PVAT hypoxia and improving the metabolic profile. In the present study, we used a nonobese prediabetic rat model with localized PVAT inflammation to test this hypothesis. Not only did Pi supplementation ameliorate PVAT inflammation, it also improved the cardiac autonomic and cerebrovascular dysfunction associated with this metabolically impaired phenotype.

## METHODS

### Experimental Animals

All animal experiments were conducted in accordance with an experimental protocol approved by our institutional Animal Care and Use Committee in complying with the National Institutes of Health's *Guide for the Care and Use of Laboratory Animals, 8th Edition*.<sup>32</sup>

Five-week-old male Sprague-Dawley rats weighing 180 to 200 g were divided into 4 groups (6 animals

each) according to the diet they were kept on. Group 1 received a control diet (normal chow: 0.75) offering 3.8 kcal/g with 0.75 mg free phosphorus per kilocalorie. The control diet composition (American Institute of Nutrition [AIN]-93 G, Table) and Pi content were based on the AIN's recommendation for adult rat maintenance diets.<sup>33</sup> Group 2 was fed a mild hypercaloric diet offering 4.5 kcal/g with 0.375 mg free phosphorus per kilocalorie (hypercaloric: 0.375). The hypercaloric diet composition was based on our previous studies showing that a 12-week feeding of an hypercaloric diet, offering  $\approx 39\%$  calories from fat with a 5% saturated fat content by weight, led to a nonobese prediabetic phenotype.<sup>13,14,18,34,35</sup> A loss of 50% of the Pi content was assumed in the previous studies because of nutrient displacement during preparation. The 2 additional groups were fed a hypercaloric diet with phosphorus content of 0.75 (Group 3; hypercaloric: 0.75) and 1.5 mg/kcal (Group 4; hypercaloric: 1.5), which are equal to and twice as much as the AIN-recommended content. Diets were prepared in house using Pi-free purified diet mix. Different amounts of potassium phosphate were added to each diet to reach the desired phosphorus levels. Diet ingredients including casein, L-methionine, cellulose, mineral mix (AIN-93G MX), Pi-free mineral mix (AIN-93G phosphorus free), vitamin mix (AIN-93VX), and potassium phosphate monobasic were obtained from Dyets (Bethlehem, PA). Detailed diet composition is shown in the Table. Animals were fed for a total of 12 weeks. Two additional groups (6 animals each) were included. The first received a hypercaloric diet with 0.375 mg phosphorus/

**Table** Rat Diet Composition

Ingredients	NC, AIN-93G, 0.75 mg/kcal	Hypercaloric, 0.37 mg/kcal	Hypercaloric, 0.75 mg/kcal	Hypercaloric, 1.5 mg/kcal
Casein	200	200	200	200
Phosphate from casein	1.52	1.52	1.52	1.52
L-methionine	3	3	3	3
Starch, 3.75 kcal/g	400	155.1	147.7	133.3
Sucrose, 3.9 kcal/g	232	150.8	150.8	150.8
Fructose, 3.68 kcal/g	0	200	200	200
Oil, 8.84 kcal/g	70	45.5	45.5	45.5
Hydrogenated vegetable oil, 8.84 kcal/g	0	150	150	150
Cellulose, 4 kcal/g	50	50	50	50
Mineral mix	35	...	...	...
Phosphate-free mineral mix	...	35	35	35
Vitamin mix	10	10	10	10
Potassium phosphate monobasic	0	0.6	8	22.4
Total weight, g	1000	1000	1000	1000
Total E kcal/g	3.8 kcal/g	4.5 kcal/g	4.5 kcal/g	4.5 kcal/g
E from fat, %	16%	39%	39%	39%

AIN indicates American Institute of Nutrition; NC, normal chow; and E, Energy.

kcal for 10 weeks and then given a hypercaloric diet with 1.5 mg phosphorus/kcal (Group 5; hypercaloric: +1.5). The second group received a control diet with low phosphorus content (0.375 mg/kcal) for 12 weeks (Group 6; normal chow: 0.375).

The main changes in calorie content between normal chow and hypercaloric diets are brought about by the addition of the hydrogenated vegetable oil simulating typical Western diets rich in refined sugars and saturated fat. Fructose is particularly enriched in prepared foods, corn syrup additives, and carbonated beverages.<sup>36,37</sup> The high fat, high fructose model was selected because it is widely used in research involving vascular and metabolic dysfunction.<sup>38–45</sup> Moreover, the high-fat, high-fructose diet was shown to culminate in a robust type 2 diabetes model in rats after prolonged feeding.<sup>43</sup> The fat content and feeding duration were modified to allow for a nonobese prediabetic phenotype at 12 weeks, which degenerated into decompensated hyperglycemia after 24 weeks of feeding.<sup>14</sup> In our hands, hyperinsulinemia, dyslipidemia, and localized adipose tissue inflammation (perivascular and perirenal) were consistent observations in the rat model receiving this diet.<sup>14,18,35,46</sup> The modification of the added amounts of starch, sucrose, and oil were necessary to maintain consistency as the amount of other semi-solids and powders changed, as well as achieve the desired calorie density.

Littermates were ordered in batches of 6, 1 rat per treatment group. Upon receipt, rats were caged individually by the animal facility technicians in cages given preassigned numbers randomly corresponding to the 6 treatment groups (each consisting of 6 rats). Animals were kept at a controlled temperature and humidity and a 12-hour light/dark cycle. Daily food intake was recorded, and calorie intake was calculated. Animals were weighed regularly, and body composition was determined using an LF10 Minispec nuclear magnetic resonance machine (Bruker, Billerica, MA). Different tissue densities were detected to measure the fat:lean ratio. The values obtained from each rat were compared with a standardized calibrated rat.

### Echocardiography and Noninvasive Hemodynamics

Following the intended feeding duration, systolic blood pressure was measured noninvasively by tail cuff using a CODA high-throughput monitor (Kent Scientific, Torrington, CT).<sup>47</sup> Any irregular or unacceptable recording noted as a false recording by the system was excluded. Additionally, echocardiography along the parasternal long axis M and B modes was done to assess heart structure and function using SonixTouch Q+ ultrasound (BK Ultrasound, Peabody, MA).

### Serum Collection and Analysis

Blood samples (0.5 mL) were collected from all rats by tail vein puncture before being euthanized. Rats were fasted in metabolic cages with free access to drinking water for 12 hours before sample collection. Blood glucose measurement was done using Accu-Chek Performa glucometer (Roche Diagnostics, Rotkreuz, Switzerland). Blood urea nitrogen, serum phosphorus, serum creatinine, serum calcium, serum magnesium, and serum triglycerides were measured using the Vitros 350 analyzer (Ortho Clinical Diagnostics, Johnson & Johnson, Buckinghamshire, UK). Rat serum levels of adiponectin, leptin, and insulin were measured using ELISA kits according to the manufacturer's protocol (Thermo Fisher Scientific, Waltham, MA).

### Tissue Collection, Invasive Hemodynamics, and Pressure Myography Experiments

At the end of 12 weeks of feeding, anesthetized rats were instrumented with catheters inserted in the carotid artery and the jugular vein for invasive hemodynamic assessment as described previously.<sup>35</sup> Briefly, mean arterial pressure (MAP) and heart rate (HR) were measured through the carotid artery catheter connected to a Millar pressure transducer to measure. Data acquisition was performed by PowerLab (AD Instruments, Dunedin, New Zealand) and recorded using LabChart Pro 8 (AD Instruments) software. After a 45-minute stabilization period, baroreceptor sensitivity was assessed by the vasoactive method as previously described.<sup>48</sup> Increasing doses of phenylephrine (0.25, 0.5, 0.75, 1, 2  $\mu$ g) and sodium nitroprusside (0.5, 1, 2, 4, 8  $\mu$ g) were injected into the jugular vein at 5-minute intervals, which were enough for MAP and HR to return to baseline values. Peak changes in MAP ( $\Delta$ MAP) and HR ( $\Delta$ HR) were recorded.  $\Delta$ HR was plotted as a function of  $\Delta$ MAP in each treatment group, and the mean slope of the linear regression of  $\Delta$ HR versus  $\Delta$ MAP together with its confidence interval and SEM were calculated using GraphPad Prism software to represent baroreflex sensitivity and compared among groups. The maximal rate of the rise of ventricular pressure, indicative of left ventricular function, was extracted from the LabChart recording.

After the experiment, anesthetized rats were euthanized by decapitation and exsanguination. The thoracic cavity was exposed for organ and tissue collection. Brainstem and PVAT (surrounding the thoracic aorta extending from the aortic arch to the diaphragm) were dissected, frozen in liquid nitrogen, and stored at  $-80^{\circ}\text{C}$ . Midsections of heart ventricles, thoracic aortic rings, as well as renal cortices were collected. Moreover, infrascapular and epididymal fat pads were dissected as examples of bona fide BAT<sup>49,50</sup> and visceral WAT,<sup>51</sup> respectively. To cover all the functional

and molecular experiments planned, rats in every group were alternated whereby heart and aortic tissues from 1 rat would be fixed in 4% formaldehyde, whereas those from the next would be frozen in liquid nitrogen and stored at  $-80^{\circ}\text{C}$  for histopathology and Western blotting experiments, respectively.

Pressure myography experiments on middle cerebral arterioles were performed as described previously.<sup>52</sup> The intravascular pressure was gradually raised in a series of steps to 10, 20, 40, 60, 80, 100, 120, and 140 mm Hg. The outer diameter of the vessel was measured at each pressure point. The pressure was then dropped back to 10 mm Hg, and the vessel was washed and kept in a calcium-free buffer containing NaCl 130 mmol/L, KCl 4 mmol/L, MgSO<sub>4</sub>·7H<sub>2</sub>O 1.2 mmol/L, NaHCO<sub>3</sub> 4 mmol/L, HEPES 10 mmol/L, KH<sub>2</sub>PO<sub>4</sub> 1.18 mmol/L, glucose 6 mmol/L, EDTA 0.03 mmol/L, and EGTA 2 mmol/L, pH 7.4, and the ramp was repeated. Active tone was calculated as the difference in the outer diameter of the middle cerebral artery when in calcium-containing and calcium-free buffer at the respective pressure points.

### Determination of PVAT Macrophage Polarization by Fluorescence-Activated Cell Sorting

Stromal vascular cells were isolated from freshly dissected PVAT as described previously.<sup>53</sup> CD45/CD68/CD86 staining was used to identify M1 polarized macrophages, whereas M2 macrophages were identified by CD45/CD68/CD163 staining.<sup>54</sup> An aliquot of the stromal fraction containing  $10^6$  cells was incubated in fluorescence-activated cell sorting buffer with 4',6'-diamidino-2-phenylindole (1:100), 1:50 APC-Cy780-conjugated anti-CD45, 1:10 phenylephrine-conjugated anti-CD68, 1:125 fluorescein isothiocyanate-conjugated anti-CD86 (Thermo Fisher Scientific), and 1:200 APC647-conjugated anti-CD163 (Bioss Antibodies, Woburn, MA) on ice for 30 minutes in the dark. Cells were gently washed 3 times and resuspended in fluorescence-activated cell sorting buffer. Stained cells were counted using a BD FACSAria Cell Sorter (BD Biosciences, San Jose, CA), and the M1 to M2 Macrophage ratio (M1/M2) was determined. Antibody-beads mixtures, fluorophore-conjugated isotypes, and unstained cells were used to set compensation and gating.

### Immunohistochemistry and Histopathology

Serial sectioning and staining of formalin-fixed heart midsection, brainstem, aortic segments, renal cortices, PVAT, epididymal, and infrascapular adipose were performed simultaneously for accurate comparison as previously described.<sup>13</sup> Hematoxylin and eosin staining

was used for gross examination of cardiac and aortic tissue structure and to compare adipocyte size in different adipose depots across treatments. Medial thickness was measured in aortic sections, whereas inter-fibrillar edema, as indicated by myocardial fiber separation in the papillary muscle, was considered indicative of possible focal ischemic injury.<sup>55</sup> Masson's trichrome staining was used to assess connective tissue fiber deposition in the heart and aorta. Renal cortical sections were stained with periodic acid Schiff stain for the examination of glomerular and mesangial matrix area alterations as previously described.<sup>18</sup> Mesangial matrix index was calculated as the ratio of the mesangial area to the glomerular area. To evaluate calcium deposition in rat kidneys, the Von Kossa stain was used as previously described.<sup>56</sup> Dihydroethidium staining was performed on cryosections to demonstrate reactive oxygen species load. Fluorescent images were obtained through an Alexa Fluor 568 filter for the dihydroethidium red fluorescence. In vascular tissue, the red fluorescence was measured against the green collagen autofluorescence obtained through the Alexa Fluor 488 filter. Immunohistochemical detection of CD68 in the heart and the ionized calcium-binding adaptor molecule 1 (IBA-1) in the brainstem was performed using 1:100 and 1:1000 concentrations of rabbit anti-CD68 and rabbit anti-IBA-1, respectively (Abcam, Cambridge, UK), and visualized using the Novolink Polymer Detection Kit (Leica Biosystems, Buffalo Grove, IL) according to the manufacturer's protocol. Control experiments were performed by omitting primary antibodies and using rabbit IgG (immunoglobulin G) controls. Images were taken using an Olympus CX41 light microscope (Olympus, Tokyo, Japan). In each representative slide, dihydroethidium fluorescence or trichrome staining was semiautomatically quantified in 20 fields and expressed as a percentage of staining of total surface area, and the results from all fields were averaged. Hematoxylin and eosin was used to assess adipocyte size and papillary edema measured by ImageJ (National Institutes of Health, Bethesda, MD). At least 10 adipocytes were measured from 5 random areas in the slide in question, and total inter-fibrillar space was calculated from heart sections. Quantification was performed by a blinded assessor via isolation and quantification of the staining intensity using ImageJ software and normalization to the tissue area in each slide.

### Cell Culture

The induction of adipogenic differentiation of human bone marrow-derived mesenchymal stem cells was done as previously described with slight modification.<sup>57</sup> Briefly, bone marrow-derived mesenchymal stem cells were seeded in 6-well plates at a density of 50 000 cells per well in Dulbecco's Modified Eagle's Medium-low glucose (DMEM-LG) containing 10% fetal

bovine serum and 1% penicillin/streptomycin and were allowed to reach 80% to 90% confluency before the induction of adipogenic differentiation. Cells were washed twice with PBS, and media was then replaced with adipogenic induction medium containing 0.1 mmol/L 3-isobutyl-1-methylxanthine, 1  $\mu$ mol/L dexamethasone, 2  $\mu$ mol/L pioglitazone, and 40 mIU/L insulin for 10 days. Adipogenic differentiation was followed visually under the microscope through the formation of intracellular lipid droplets. Adipogenic induction medium was then replaced with maintenance media containing 40 mIU/L insulin and 2  $\mu$ mol/L pioglitazone for 5 days. Following adipogenic differentiation, adipocytes were incubated with either DMEM-LG (1 mmol/L Pi) or phosphate-supplemented DMEM-LG (4 mmol/L Pi) for 24 hours. The 4-fold increase was meant to simulate the increase of Pi intake in a hypercaloric diet from 0.375 mg/kcal to 1.5 mg/kcal used in the *in vivo* experiment. Thereafter, cells were either incubated with DMEM-LG or DMEM-LG containing 1.6 mmol/L palmitic acid and 40 mIU/L insulin for 24 hours in the continued presence of 4 mmol/L Pi added as monobasic sodium phosphate, with the final medium pH adjusted to 7.4. At this stage, adipocytes were cocultured with THP-1 human leukemic monocytes (primarily cultured in Roswell Park Memorial Institute (RPMI) medium containing 10% fetal bovine serum and 1% penicillin/streptomycin) at a density of 50 000 cells per well for an extra 24 hours, following which cells were lysed, and protein was extracted as described below. In other experiments, cells were trypsinized, stained with anti-CD45 and anti-CD86, and subjected to fluorescence-activated cell sorting as described above. For the THP-1 adhesion assay, adipocytes were seeded into a 96-well plate at a concentration of 5000 cells per well and were left to attach for 24 hours and then exposed to either normal medium or the medium containing 1.6 mmol/L palmitic acid and 40 mIU/L insulin. THP-1 cells labeled with Hoescht molecular probes stain (Nuc Blue; Sigma) were added at a density of 20 000 cells per well into each well. After 30 minutes incubation time at 37 °C, the THP-1-containing medium was aspirated and the wells washed twice with PBS 1X (Sigma). Images of the adherent cells were later taken using a Zeiss Axio microscope at the same excitation/emission spectra for monocytes, and superimposed on brightfield images to visualize the nonlabeled cells.

### Western Blotting

Experiments were performed as described previously.<sup>52,58</sup> PVAT, epididymal, and infrascapular adipose tissue samples were homogenized on ice, and the protein extracts were separated by SDS-PAGE. Proteins were then blotted to nitrocellulose membranes and were incubated in primary antibodies (1:500 for rabbit polyclonal anti-IL-1 $\beta$  [interleukin-1 $\beta$ ], 1:1000 for rabbit monoclonal anti-GAPDH, rabbit polyclonal anti-HIF-1 $\alpha$  [anti-hypoxia

inducible factor-1 $\alpha$ ] [Abcam], and rabbit polyclonal anti-UCP1 [Cell Signaling, Danvers, MA]) overnight at 4 °C. Membranes were then washed with 0.02% Tris-buffered saline with 0.1% Tween 20, and incubated for 1 hour at room temperature in 1:40 000 biotinylated conjugated goat anti-rabbit immunoglobulin. Membranes were then washed and incubated for 30 minutes at room temperature with 1:200 000 horseradish peroxidase-conjugated streptavidin (Abcam). After 2 washes with 0.02% Tris-buffered saline with 0.1% Tween 20 (5 minutes) and 2 washes with Tris-buffered saline (5 minutes), the blots were exposed to Clarity Western enhanced chemiluminescence substrate (BioRad, Hercules, CA) for 5 minutes and then detected by the Chemidoc imaging system (BioRad). Densitometric analysis of the protein bands was performed using ImageJ software. Measurements were normalized to the density of GAPDH.

All chemicals were obtained from Sigma (St. Louis, MO) unless otherwise indicated.

### Statistical Analysis

Data were expressed as mean $\pm$ SEM. Comparisons among groups were done using 1-way or 2-way ANOVA followed by the appropriate post hoc test as indicated in the corresponding section in the Results or the figure legends. Whenever repeated measurements were made from the same animal (at different dosing or pressure levels), a repeated measures analysis (in the dosing or pressure factor) was used (Figures 3, 6, and 8). Linear regression was used to evaluate baroreflex sensitivity. GraphPad Prism version 7 software was used for statistical analysis. A *P* value <0.05 was considered statistically significant. Statistical analysis was done once comparing data from all groups. However, for ease of presentation of results, the figures were broken down to facilitate the depiction of the effect of different treatment groups. In this arrangement, normal chow and hypercaloric (0.375 mg/kcal phosphorus) data appear in multiple figures, yet statistical tests were only conducted once.

### Availability of Data and Materials

All data generated or analyzed during this study are included in this published article.

## RESULTS

### Metabolic and Gross Hemodynamic Impact of Hypercaloric Feeding With Different Levels of Phosphorus

The metabolic and gross hemodynamic profile of rats fed a hypercaloric diet with low Pi has been characterized in our previous work.<sup>14,18,34</sup> The present study showed similar results with an increased cumulative

calorie intake that is equivalent to the previously observed daily increase of  $\approx 14$  kcal (Figures S1A). This occurred in the absence of increased body weight or fasting blood glucose level (Figures S1B and S1C). As for noninvasive hemodynamic measurements, no changes in systolic blood pressure and ejection fraction were detected (Figures S1G and S1H). As previously observed, hypercaloric-fed rats demonstrated an increased adiposity as indicated by an elevated fat:lean ratio, which was not affected by different levels of Pi supplementation (Figure S1D). On the other hand, the characteristic increase in serum triglycerides that appeared in this model of early metabolic challenge was reversed by Pi supplementation at both 0.75 and 1.5 mg/kcal (Figure S1E). Moreover, although the 0.75 mg/kcal supplementation level did not affect the elevated serum insulin levels in hypercaloric-fed rats, supplementation at 1.5 mg/kcal appeared to be associated with fasting serum insulin levels that were not different from those in control rats (Figure S1F). Interestingly, despite the observed increase in adiposity, serum concentrations of leptin and adiponectin did not appear to vary in different rat groups (Figures S1H and S1I). Significantly, despite a trend to increase, serum Pi levels in rats receiving the hypercaloric diet deficient in Pi was not different from that in rats receiving the control diet or the hypercaloric diet with the intermediate Pi dose of 0.75 mg/kcal (Figure S2A). Importantly though, rats receiving the hypercaloric diet supplemented by 1.5 mg/kcal Pi had serum levels that were significantly less compared with those with a Pi-deficient diet. Moreover, the different rat groups showed similar serum concentrations of calcium (Figure S2B) and magnesium (Figure S2C). Interestingly, the general trends observed after the 12-week feeding period were preserved, albeit with lesser differences at the earlier time point of 8 weeks (Figure S3), indicating a consistent trajectory over the feeding period.

### Impact of Phosphorus Supplementation on Markers of Adipose Tissue Inflammation in Hypercaloric-Fed Rats and In Vitro in Cultured Adipocytes

Our previous studies showed that hypercaloric feeding was associated with increased UCP1 expression in PVAT but not in other adipose depots, which was accompanied by increased markers of hypoxia and inflammation.<sup>14</sup> Similar findings were obtained in the present study, whereby an hypercaloric: 0.375 Pi diet was found to induce an increased UCP1 expression with parallel increases in HIF-1 $\alpha$  and IL-1 $\beta$  (Figure 1A). Pi supplementation led to a dose-dependent decrease in UCP1 PVAT expression. Parallel reduction in HIF-1 $\alpha$  and IL-1 $\beta$  expression was seen particularly with the 1.5 mg/kcal Pi dose (Figure 1A). Interestingly, although PVAT adipocyte size increased upon hypercaloric

feeding, Pi supplementation led to a reversal of this effect (Figure 1B). Upon examination of the impact of dietary changes on bona fide WAT and BAT, UCP1 expression was not detected and did not change in epididymal and infrascapular adipose tissue, respectively (Figure 1C and 1E). In parallel, HIF-1 $\alpha$  expression did not change in either tissue with any of the diets, whereas no IL-1 $\beta$  expression was seen (Figure 1C and 1E). Nevertheless, an increase adipocyte size was observed in both WAT and BAT representative tissues from rats fed a hypercaloric: 0.375 Pi diet. This change was reversed with Pi supplementation, particularly at the 1.5 mg/kcal dose (Figure 1D and 1F).

In an attempt to establish a direct effect of Pi on PVAT changes, we have developed an in vitro cell culture model to simulate the inflammatory changes occurring upon exposure to increased calorie intake and hyperinsulinemia. Adipocytes differentiated from human bone marrow-derived mesenchymal stem cells showed lipid droplet accumulation and UCP1 expression (Figure S4A and S4B). Differentiated adipocytes stressed by exposure to 40  $\mu$ M and 1.6 mmol/L palmitic acid appeared to develop a phenotype that favors inflammation demonstrated by increased THP-1 monocyte adhesion compared with adipocytes incubated in control media (Figure S4C). The adherent monocytes developed macrophage markers indicative of initiation of inflammatory response (Figure S4D). Interestingly, HIF-1 $\alpha$  and IL-1 $\beta$  expression levels increased in the stressed adipocytes exposed to THP-1 monocytes as observed in the PVAT of prediabetic rats receiving hypercaloric: 0.375 (Figure 1G). Significantly, when this experiment was repeated in 4 mmol/L Pi, the increase in the expression of both HIF-1 $\alpha$  and IL-1 $\beta$  was attenuated.

### Phosphorus Supplementation Ameliorates Hypercaloric-Induced Alteration of PVAT Macrophage Polarization

Resident macrophages contribute to adipose tissue homeostasis by adopting a wide range of activation phenotypes within the M1/M2 model of polarization. Although M2 polarization is prevalent in a healthy adipose tissue, obesity and adipose expansion tend to alter the macrophages toward the M1 polarization concomitant with adipose tissue inflammation.<sup>59</sup> In line with the inflammatory changes, flow cytometric examination of the stromal vascular cell fraction of PVAT for macrophage markers showed that the ratio of CD45<sup>+</sup>/CD68<sup>+</sup>/CD86<sup>+</sup> cells corresponding to M1 polarized macrophages to the CD45<sup>+</sup>/CD68<sup>+</sup>/CD163<sup>+</sup> corresponding to M2 cells increased in animals receiving a low-Pi hypercaloric diet (Figure 2A and 2B). Importantly, parallel decreases in M1/M2 cell ratio were seen in PVAT from rats fed a hypercaloric diet with 0.75 and 1.5 mg/kcal Pi (Figure 2C and 2D). Results of the

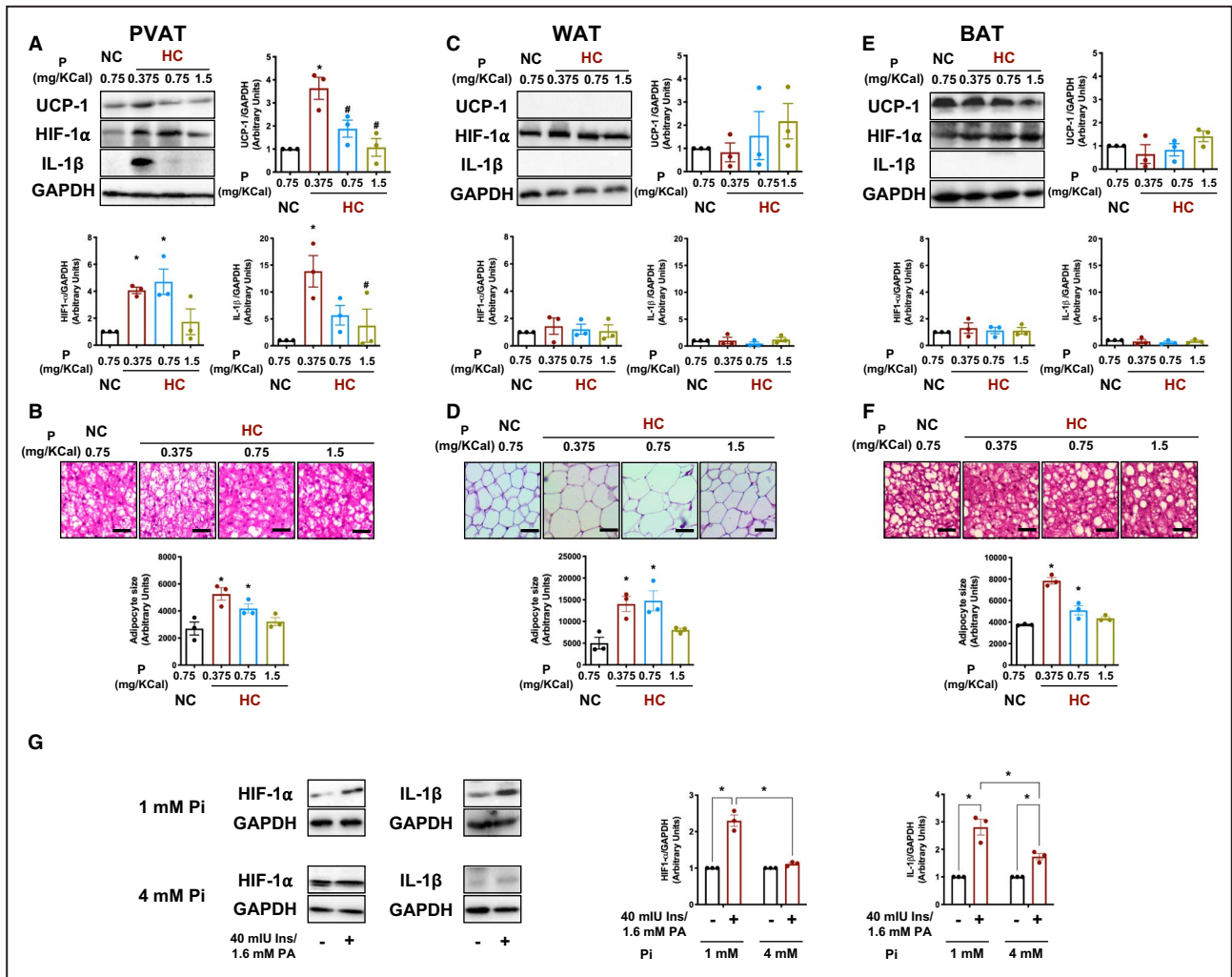


**Figure 1.** Manifestations of perivascular adipose tissue (PVAT) inflammation in hypercaloric (HC)-fed rats compared with changes in a visceral white adipose tissue (WAT) and brown adipose tissue (BAT) pools and the ameliorative effect of inorganic phosphate (Pi) supplementation.

**A, C, and E,** Representative Western blotting (top left) and summary of the quantified data (top right and bottom) showing the expression levels of UCP1 (uncoupling protein 1), HIF-1 $\alpha$  (hypoxia-inducible factor-1 $\alpha$ ), and IL-1 $\beta$  (interleukin-1 $\beta$ ) in PVAT, epididymal WAT, and infrascapular BAT, respectively, of normal chow (NC)- (Group 1) and HC-fed rats with different concentrations of phosphorus (P) supplementation (Groups 2, 3, and 4). **B, D, and F,** Representative micrographs (top) and summary of the quantified data (bottom) showing the adipocyte size in hematoxylin and eosin–stained PVAT epididymal WAT and infrascapular BAT sections, respectively. Scale bars are 25  $\mu$ m. **G,** Representative Western blotting (left) and summary of the quantified data (right) showing the expression levels HIF-1 $\alpha$  and IL-1 $\beta$  in cultured adipocytes differentiated from mesenchymal stem cells at 1 and 4 mmol/L P in culture media with or without insulin (Ins) and palmitic acid (PA) challenge. The blots shown are representatives of experiments on tissues from 3 different sets of rats, whereas summary data for micrographs are obtained from 9 sections from 3 different rats per group. Results shown are mean $\pm$ SEM. Statistical significance was tested by 1-way ANOVA followed by Tukey multiple comparisons test for **A** through **F**, and 2-way ANOVA followed by Sidak post hoc test for **G**. \*Denotes a *P* value <0.05 vs NC-fed rat values. BAT indicates brown adipose tissue; GAPDH, glyceraldehyde-3-phosphate dehydrogenase; HC, hypercaloric chow; HIF-1 $\alpha$ , hypoxia inducible factor-1 $\alpha$ ; IL-1 $\beta$ , interleukin 1 $\beta$ ; NC, normal chow; PVAT, perivascular adipose tissue; UCP1, uncoupling protein 1; and WAT, white adipose tissue.

fluorescence-activated cell sorting experiments are summarized in Figure 2E.

### Impact of Dietary Phosphorus on Metabolic Efficiency and Protein Metabolism

Metabolic efficiency (weight gained in grams per kilocalorie of energy intake) was assessed for every rat in

the different diet groups as a measure of energy stored somatically versus that dissipated by mitochondrial uncoupling.<sup>60</sup> As could be inferred from the increased energy intake without an equivalent rise in body weight, energy efficiency decreased in rats receiving a hypercaloric: 0.375 Pi diet (Figure S5A). Consistent with the putative UCP1 inhibitory effect, energy efficiency increased in rats receiving a Pi-supplemented hypercaloric diet



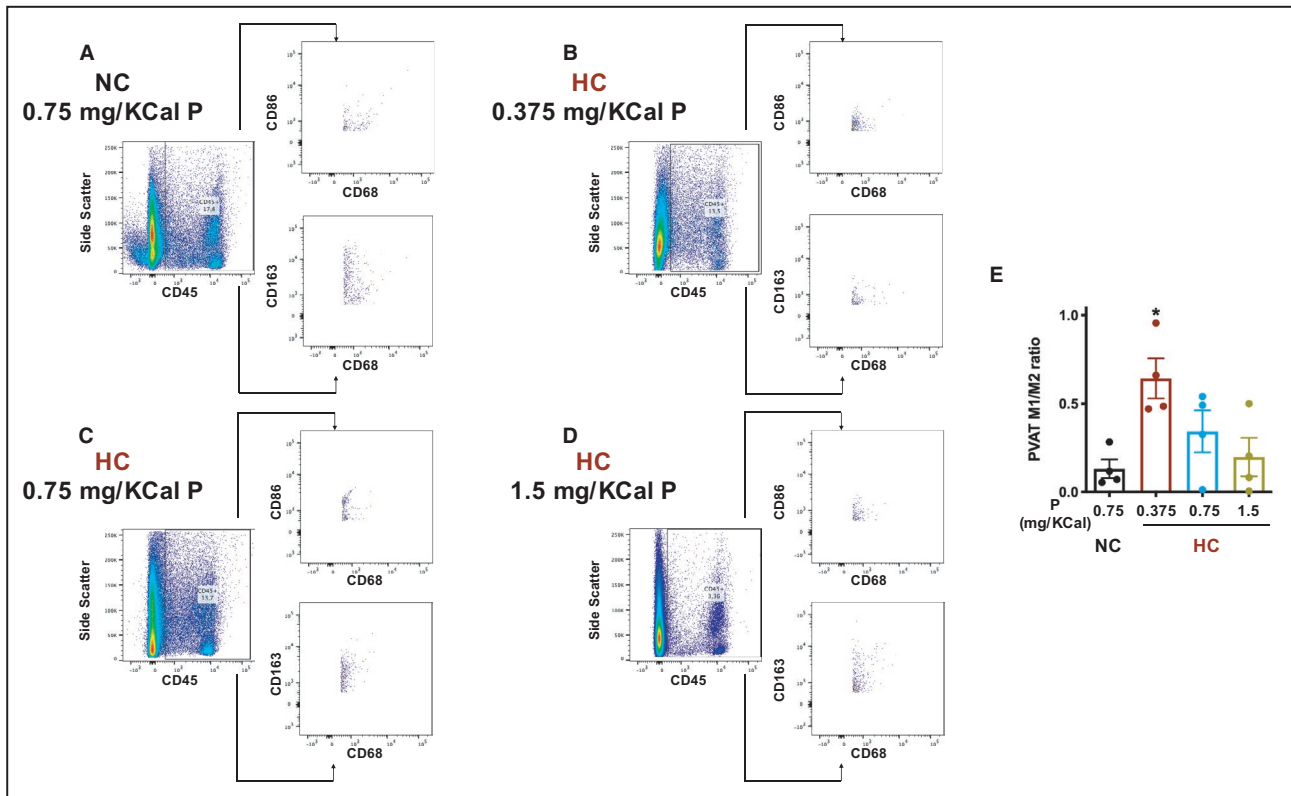


**Figure 2. Phosphorus supplementation restores perivascular adipose tissue (PVAT) macrophage polarization in rats fed a hypercaloric (HC) diet.**

**A** through **D**, Representative fluorescence-activated cell sorting scattergrams showing PVAT leukocytes expressing M1 vs M2 polarized macrophages using polarization markers in rats fed normal chow (NC; Group 1) or an HC diet with different inorganic phosphorus (P) concentrations (Groups 2, 3, and 4). **E**, Summary of the ratio of M1/M2 PVAT macrophages from 4 different animals per group. Results shown are mean $\pm$ SEM. Statistical significance was tested by 1-way ANOVA followed by Tukey multiple comparisons test. \*Denotes a P value <0.05 vs NC-fed rat values. HC indicates hypercaloric chow; M1/M2, M1 to M2 macrophage ratio; NC, normal chow; and PVAT, perivascular adipose tissue.

(Figure S5A). Interestingly, this reduced energy efficiency did not appear to be associated with increased protein metabolism, because blood urea nitrogen did not change among control and hypercaloric-fed rat groups at different Pi levels (Figure S5B).

### Phosphorus Supplementation Reverses Cardiac Autonomic Neuropathy in Hypercaloric-Fed Rats

PVAT inflammation in the nonobese prediabetic state induced by 12-week hypercaloric-diet feeding was consistently shown to be associated with parasympathetic cardiac autonomic neuropathy manifesting as a blunting of the bradycardic baroreflex in response to vasopressors.<sup>13,35</sup> This was the case in rats fed a low-Pi hypercaloric diet. An increased pressor effect was observed in these rats in response to increasing phenylephrine doses compared with rats on the control diet (Figure 3A and 3B), which is in line with the reported increased vascular contractility at this stage.<sup>14</sup> This was accompanied with an attenuation of the

bradycardic response (Figure 3C). Significantly, both effects were ameliorated in rats fed a hypercaloric diet supplemented with 1.5 mg/kcal Pi. Restoration of parasympathetic autonomic function was confirmed by examination of the baroreceptor sensitivity in response to phenylephrine (Figure 3D). Whereas the slope of the  $\Delta$ HR versus  $\Delta$ MAP line was blunted in the low-Pi hypercaloric-fed group, an increased sensitivity was observed in the 1.5 mg/kcal supplemented hypercaloric group (Figure 3E). As observed previously, no change in the sympathetic arm of the baroreflex was observed following hypercaloric feeding or after Pi supplementation (data not shown).

### Phosphorus Supplementation Alleviates Signs of Cardiovascular Deterioration

Histochemical examination of heart midsection from low-Pi hypercaloric-fed rats showed signs of focal injury demonstrated by an elevated papillary muscle edema, as well as increased fibrosis, macrophage infiltration, and oxidative stress (Figure 4A through

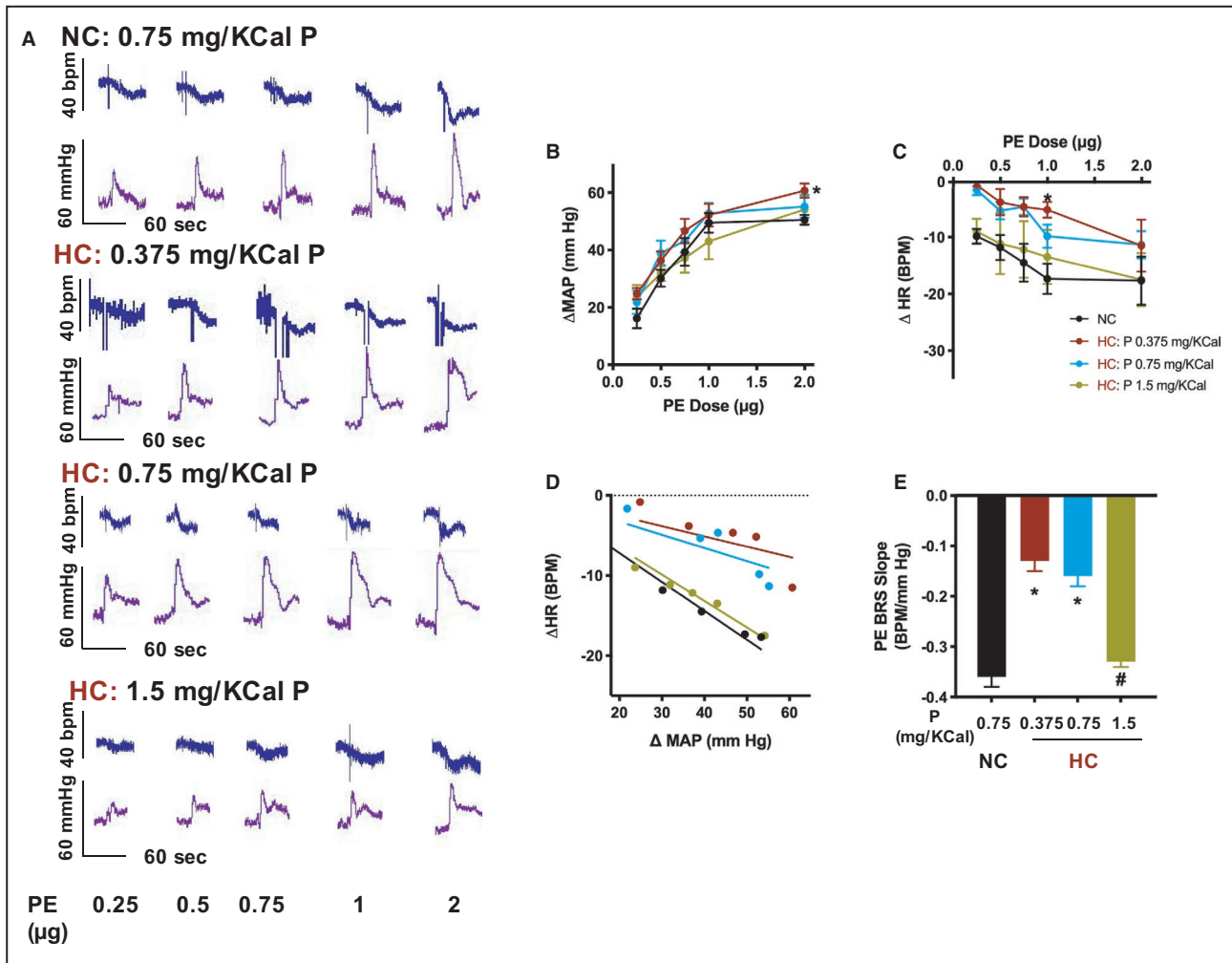


**Figure 3. Phosphorus supplementation of hypercaloric (HC) diet restores parasympathetic cardiac autonomic function.** **A**, Representative tracings of pressor (mean arterial pressure [MAP]) and cardiac (heart rate [HR]) responses to increasing phenylephrine (PE) doses in normal chow (NC)- (Group 1) and HC-fed rats with different concentrations of phosphorus (P) supplementation (Groups 2, 3, and 4). Vertical scale bars represent MAP (60 mm Hg) and HR (40 bpm), whereas horizontal scale bars represent time (60 seconds). **B**, The pressor responses to increasing doses of PE. **C**, Reflex bradycardic responses to increasing blood pressure. **D**, Best fit regression line for the correlation between ΔMAP and reflex changes in HR in response to increasing doses of PE in NC- and HC-fed rats with different concentrations of P supplementation. **E**, Slope of the linear regression of the relationship between ΔHR and ΔMAP reflecting parasympathetic baroreceptor sensitivity (BRS). Depicted data represent mean±SEM of values obtained from 6 rats per group. Statistical analysis was done by 2-way ANOVA with repeated measures in the dose factor, followed by Sidak's multiple comparisons test for (B) and (C), and 1-way ANOVA followed by Tukey multiple comparisons test for (E). \* and # denote P<0.05 vs NC and HC: 0.375 mg/kcal P, respectively. BRS indicates baroreceptor sensitivity; HC, hypercaloric chow; HR, heart rate; MAP, mean arterial pressure; NC, normal chow; and PE, phenylephrine.

4E). Pi supplementation appeared to have reversed these changes in a dose-dependent manner, with the 1.5 mg/kcal dose being consistently effective. In parallel, the low-Pi hypercaloric-induced impairment of ventricular function shown as a decreased rate of the rise of ventricular pressure was mitigated in rats fed a Pi-supplemented hypercaloric diet (Figure 4F). On the other hand, similar changes were observed for aortic tissue. Although a low-Pi hypercaloric feeding led to increased aortic medial thickness, fibrosis, and oxidative stress, Pi supplementation, particularly the

1.5 mg/kcal dose, was able to reverse these changes. Representative micrographs are shown in Figure 5A and summary data in Figure 5B through 5D.

### Phosphorus Supplementation Ameliorates Hypercaloric Diet-Induced Cerebrovascular Dysfunction and the Associated Brainstem Changes

Consistent with our previous results,<sup>34</sup> hypercaloric feeding was associated with increased cerebrovascular

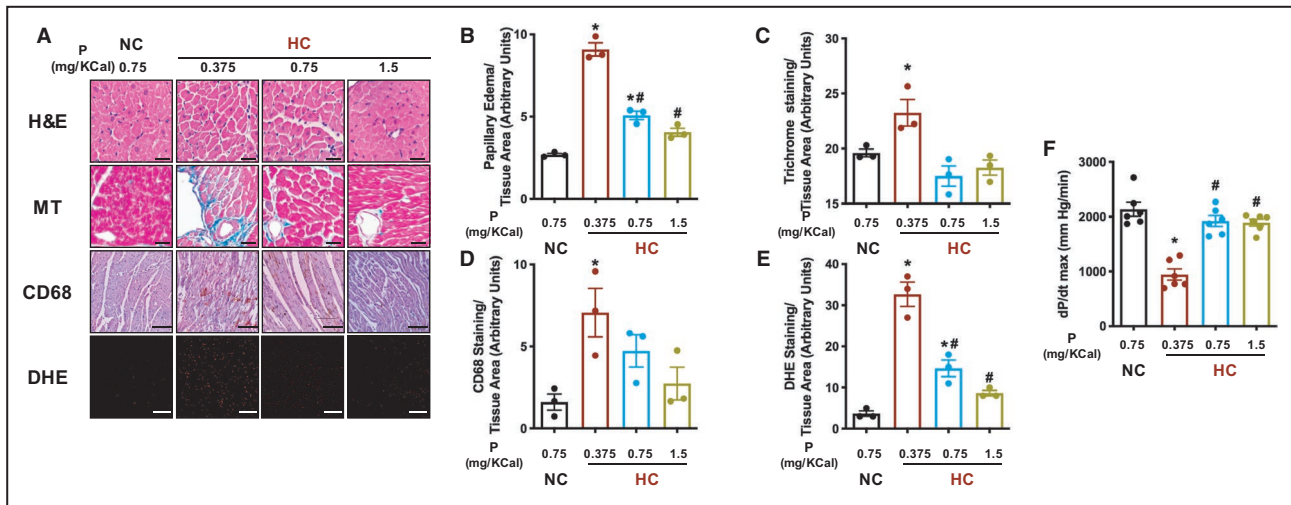


**Figure 4.** Impact of inorganic phosphorus (P) supplementation on histopathological and molecular signs of cardiac impairment induced by hypercaloric (HC) feeding.

**A,** Representative micrographs of histopathological, immunohistochemical, and dihydroethidium (DHE) staining in heart midsection of normal chow (NC)- (Group 1) and HC-fed rats with different concentrations of P supplementation (Groups 2, 3, and 4). Data presented are serial sections taken from the same tissues and are representative of 9 sections from 3 different rats in each group. Scale bars are (top to bottom): 25, 25, 50, and 50  $\mu$ m. Fibrotic staining appears as a blue color on a red background, CD68 staining appears as a brown color on a background of hematoxylin and eosin counter stain, whereas DHE staining appears as red fluorescence on a black background. Quantification values of area of interfibrillar edema (**B**), as well as the intensity of Masson trichrome (**C**), CD68 (**D**), and DHE (**E**) staining normalized to ventricular tissue area. **F,** Cardiac contractility assessed by maximal rate of rise of ventricular pressure ( $dP/dt_{max}$ ). Statistical significance was determined by ANOVA followed by Tukey post hoc test. \* and # denote  $P < 0.05$  compared with NC and HC: 0.375 mg/kcal rats, respectively. DHE indicates dihydroethidium stain; HC, hypercaloric chow; H & E, hematoxylin and eosin; MT, Masson's trichrome stain; and NC, normal chow.

myogenic tone (Figure 6A and 6B). Such an increased cerebrovascular reactivity within the operational pressure range of the middle cerebral arteriole was associated with cerebral hypoxia and increased neuroinflammation.<sup>34</sup> This was the case in hypercaloric-fed rats showing increased oxidative stress and IBA-1 staining indicative of microglial activation in the brain stem (Figure 6C). Interestingly, consistent with its effect on PVAT inflammation, cardiac autonomic and cardiovascular functions, Pi supplementation reduced the cerebrovascular tone and the associated brainstem oxidative stress and microglial activation (Figure 6D and 6E).

### Hypercaloric Intake, Rather Than Phosphorus Deficiency, Precipitates PVAT, Metabolic, and Cardiovascular Alterations, Which Can Be Reversed Upon Reinstating Dietary Phosphorus

To examine whether PVAT inflammation and the associated cardiovascular changes in rats fed a hypercaloric diet occur because of increased calorie intake or Pi deficiency, an additional group of rats fed a control diet with a Pi concentration equivalent to that in a hypercaloric diet (0.375 mg/kcal) was used. Moreover, the impact of Pi reinstatement after a 10-week exposure to a low-Pi hypercaloric diet was examined by switching these rats

to a hypercaloric diet supplemented with 1.5 mg/kcal Pi for the last 2 weeks of the feeding duration. Figure S6 depicts the gross hemodynamic and metabolic outcome of these protocols compared with rats fed a control and low-Pi hypercaloric diet for 12 weeks. Although rats in the hypercaloric diet with Pi reinstatement consumed more calories as expected, those on a low-Pi control diet did not (Figure S6A). Whereas these dietary manipulations had no bearing on body weight, blood glucose level, blood pressure, and ejection fraction (Figure S6B, S6C, S6G and S6H), only hypercaloric-fed rats with Pi reinstatement had an increased adiposity and serum insulin similar to those in rats on a low-Pi hypercaloric-fed diet. (Figure S6D and S6F). Moreover, a 2-week reinstatement of Pi at the 1.5 mg/kcal dose did not appear to alter metabolic efficiency of low-Pi hypercaloric-fed rats (Figure S6I). However, despite the lack of effect on insulin, Pi reintroduction reduced serum triglyceride levels. Serum triglyceride levels in rats fed a low-Pi control chow were also comparable to those in rats receiving a control diet with normal Pi content (Figure S6E). Serum Pi, calcium, and magnesium levels in the low-Pi control diet group and those in the Pi-reinstatement group were not different from either the control diet or Pi-deficient hypercaloric diet groups (Figure S7). Significantly, although Pi reinstatement on top of a hypercaloric diet improved ventricular function as measured by rate of

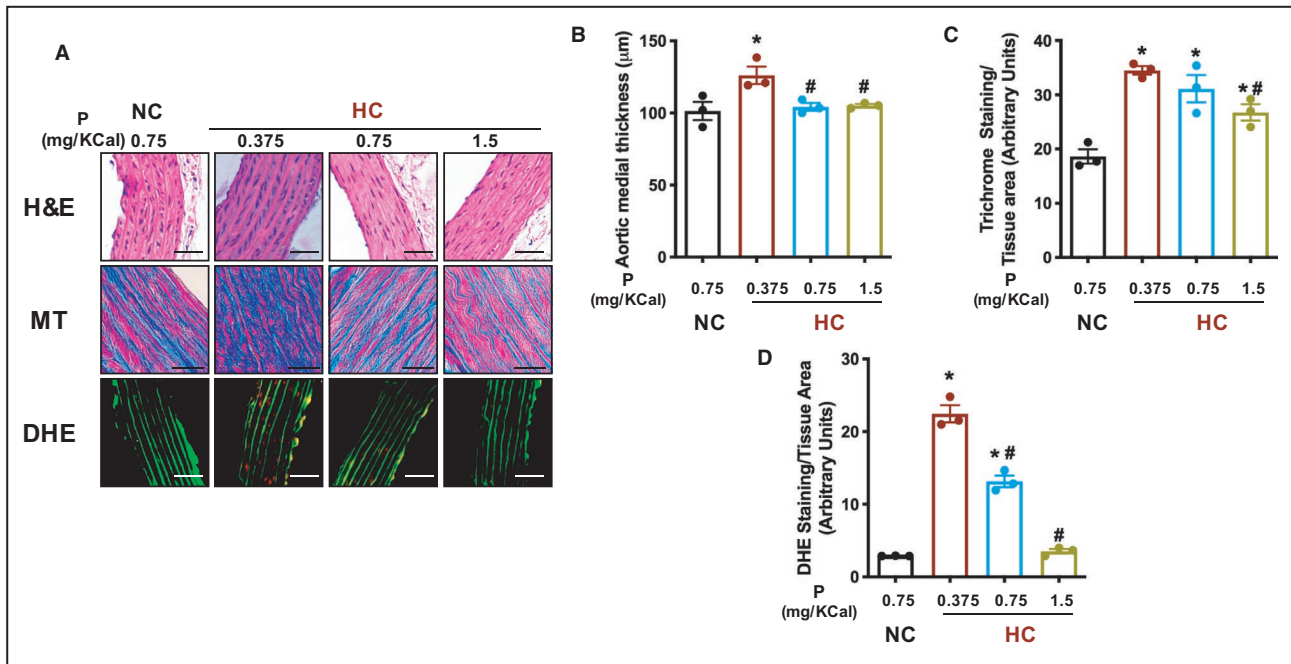


**Figure 5.** Impact of inorganic phosphorus (P) supplementation on histopathological and molecular signs of vascular impairment induced by hypercaloric (HC) feeding.

**A,** Representative micrographs of histopathological and dihydroethidium (DHE) staining in aortas of normal chow (NC)- (Group 1) and HC-fed rats with different concentrations of P supplementation (Groups 2, 3, and 4). Data presented are serial sections taken from the same tissues and are representative of 9 sections from 3 different rats in each group. Scale bars are (top to bottom): 50, 25, and 50 μm. Fibrotic staining appears as a blue color on a red background, whereas DHE staining appears as red fluorescence on a background of green collagen autofluorescence. Quantification values of medial thickness (**B**), as well as the intensity of Masson trichrome (**C**) and DHE (**D**) staining normalized to aortic tissue area. Statistical significance was determined by ANOVA followed by Tukey post hoc test. \* and # denote  $P < 0.05$  compared with NC and HC: 0.375 mg/kcal rats, respectively. H&E indicates hematoxylin and eosin. DHE indicates dihydroethidium stain; HC, hypercaloric chow; H & E, hematoxylin and eosin; MT, Masson's trichrome stain; and NC, normal chow.

the rise of ventricular pressure, rats on a low-Pi control diet appeared to have a reduced ventricular contractility (Figure S6J).

From a different perspective, molecular examination revealed no signs of PVAT inflammation in either rat group. UCP1 and HIF-1α PVAT expression levels were similar both in rats fed hypercaloric: 0.375 and receiving a 2-week 1.5 mg/kcal Pi supplementation as well as those receiving the low-Pi control diet compared with control rats (Figure 7A). PVAT IL-1β levels were low in both groups and no different from those in rats receiving control chow (Figure 7A). As opposed to rats receiving a 1.5-mg/kcal Pi-supplemented hypercaloric diet for the full duration, those in which Pi was reintroduced for the last 2 weeks of feeding showed increased PVAT adipocyte size. No such increase was seen in rats fed a low-Pi control diet (Figure 7B).

The lack on inflammatory changes in PVAT of these rats reflected on the histological and molecular markers of cardiac and vascular damage elevated in rats fed an hypercaloric: 0.375 Pi diet. No signs of papillary muscle focal injury, cardiac fibrosis, macrophage infiltration, and oxidative stress were seen in heart midsections of either rat groups (Figure 7C). Similarly, aortic intimal thickness,

trichrome, and dihydroethidium staining were within the same levels as in rats receiving a control diet with standard phosphate content (Figure 7D).

On the other hand, although increased vascular contractility in response to phenylephrine lingered in both groups, the lack of Pi in the control diet did not seem to induce parasympathetic autonomic neuropathy, and Pi reinstatement reversed the bradycardic reflex blunting induced by a hypercaloric: 0.375 Pi diet feeding as evident from the baroreflex slopes (Figure 8B). The correction of parasympathetic neuropathy could be related to the lack of signs of brainstem neuroinflammation. Both IBA-1 and dihydroethidium staining were at levels similar to control rats in both groups (Figure 8C and 8D).

### Dietary Interventions With Different Phosphorus Levels Do Not Appear to Induce Renal Structural or Functional Alterations

Increased dietary Pi carries the risk of renal damage characterized by tubular necrosis and calcium phosphate deposition.<sup>61</sup> To investigate whether the Pi amounts used in the present study induced renal changes, we have

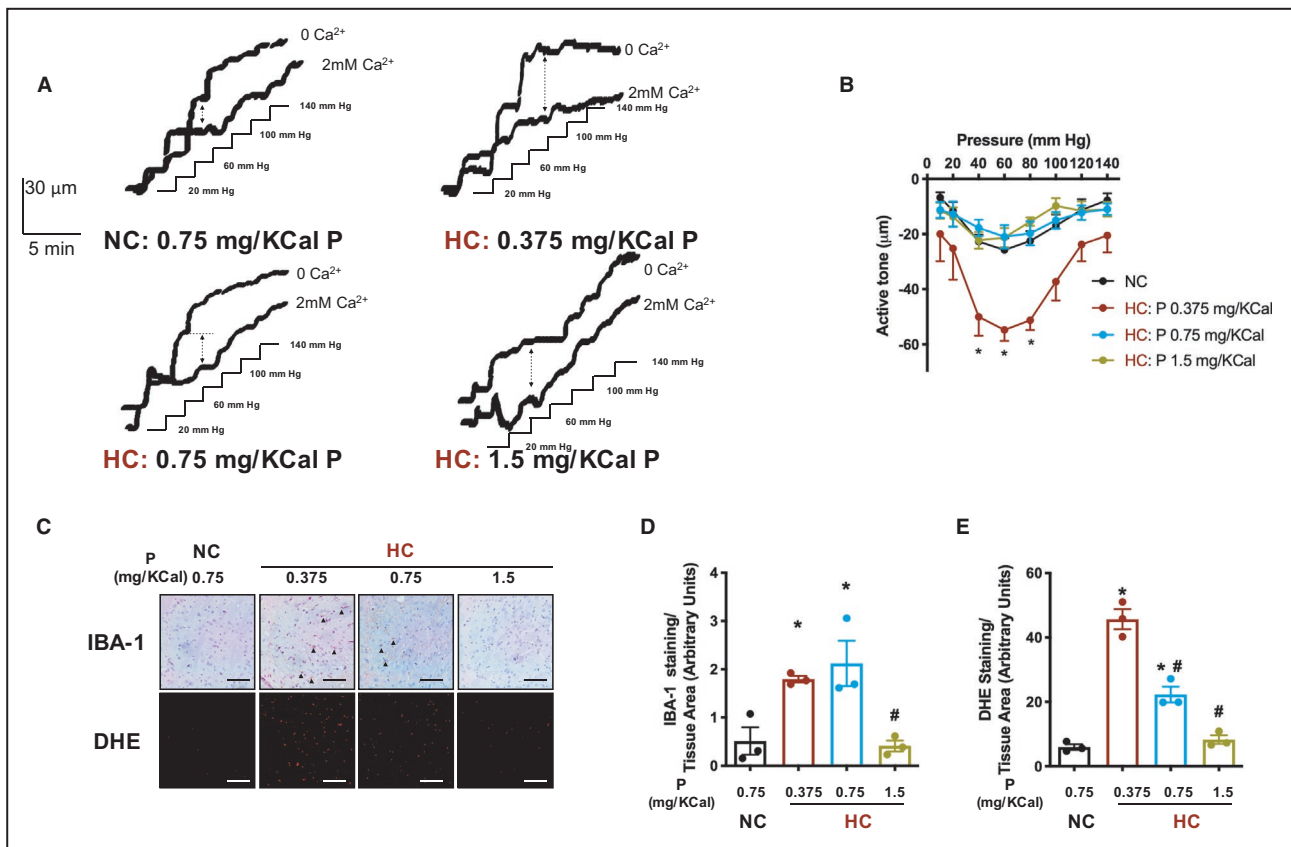


**Figure 6. Inorganic phosphorus (P) supplementation reverses cerebrovascular hypercontractility and brainstem inflammation induced by hypercaloric (HC) feeding.**

**A**, Representative tracings of pressure myography experiments depicting changes in rat middle cerebral artery diameter as a function of change in intravascular pressure in vessel segments from normal chow (NC)- (Group 1) (top left), HC: 0.375 mg/kcal P-fed (Group 2) (top right), HC: 0.75 mg/kcal P-fed (Group 3) (bottom left), and HC: 1.5 mg/kcal P-fed (Group 4) (bottom right) rats in presence (2 mmol/L Ca) and absence of calcium in the bath solution. **B**, Active tone generated by rat middle cerebral artery in vessel segments a function of pressure change ( $n=4$ ). Active tone is the difference in diameter of the vessel at a given intravascular pressure value in the absence and presence of calcium as indicated by the double-headed arrow on the tracings at 60 mm Hg. **C**, Representative micrographs of IBA-1 immunohistochemical and dihydroethidium (DHE) staining in brainstems of NC- and HC-fed rats with different concentrations of P supplementation. Data presented are serial sections taken from the same tissues and are representative of 9 sections from 3 different rats in each group. Scale bars are 100  $\mu\text{m}$ . IBA-1 staining appears as a brown color on a background of hematoxylin and eosin counter stain, whereas DHE staining appears as red fluorescence on a black background. Quantification values of IBA-1 staining are shown (**D**), as well as the intensity of DHE staining (**E**) normalized to brainstem tissue area. Statistical significance was determined by 2-way ANOVA with repeated measures in the pressure factor followed by Sidak post hoc test for (**B**) and 1-way ANOVA followed by Tukey post hoc test for (**D**) and (**E**). \* and # denote  $P<0.05$  compared with NC and HC: 0.375 mg/kcal rats, respectively. DHE indicates dihydroethidium stain; HC, hypercaloric chow; IBA-1, ionized calcium-binding adaptor molecule 1; and NC, normal chow.

undergone histological examination of kidneys from all groups. Periodic acid Schiff staining demonstrated no changes in tubular or glomerular structure (Figure S8). Similarly, von Kossa staining showed no calcium deposits in the renal cortices of kidneys from rats in different groups (Figure S8). Moreover, no differences in serum creatinine concentrations were detected among any of the treatment groups (Figure S8).

## DISCUSSION

The complexity of the pathophysiology linking metabolic dysfunction in type 2 diabetes to cardiovascular

complications has long been recognized to extend beyond simple perturbations of blood glucose and lipid levels.<sup>62</sup> However, it was not until fairly recently that investigation of pharmacological therapies for metabolic disease focused on their cardiovascular benefits as desirable outcomes, independent of their impact on hyperglycemia and blood lipid levels.<sup>63–65</sup> Although undoubtedly useful, these drugs were originally designed as hypoglycemic tools. Despite the long standing and exponentially growing evidence implicating the involvement of inflammation, particularly that in adipose tissue, in the cardiometabolic complications, direct interventions with this pathology have

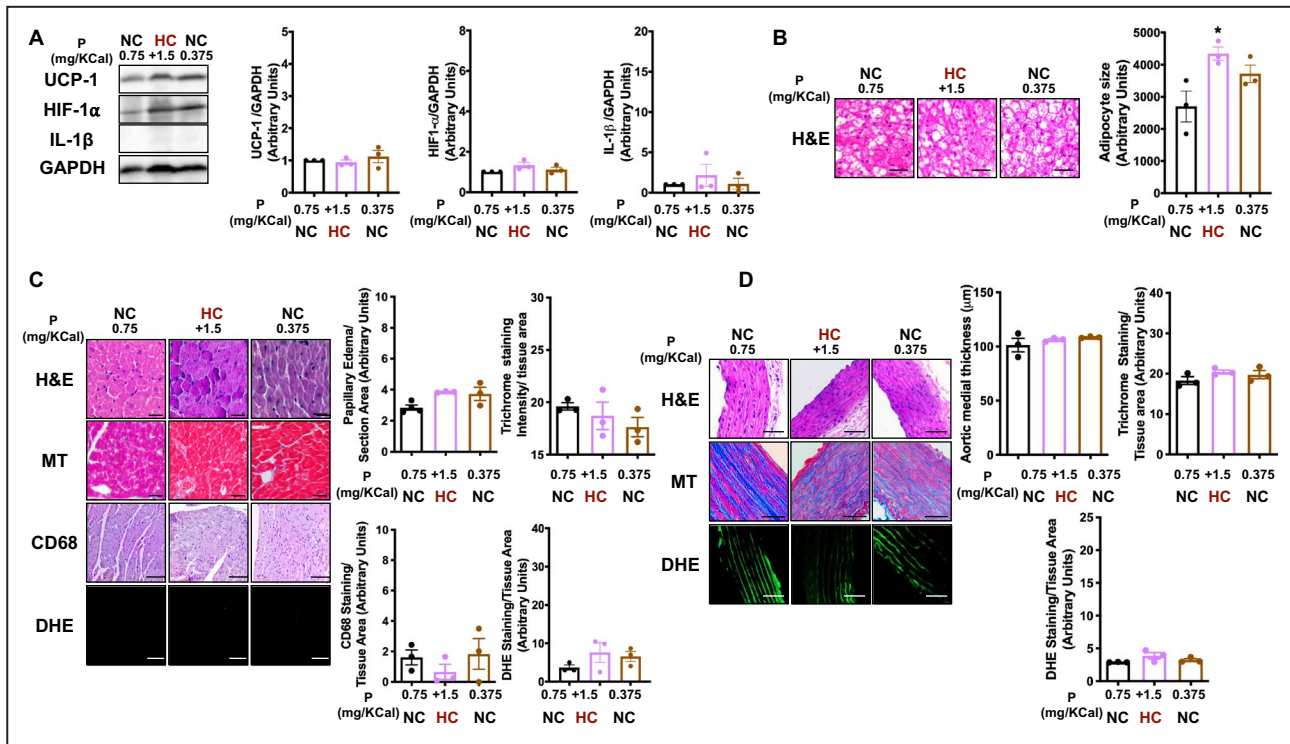


**Figure 7. Molecular and histopathological impact of low phosphorus (P) control diet feeding or P reinstatement after a 10-week, high-calorie, P-deficient diet feeding.**

**A**, Representative Western blotting (left) and summary of the quantified data (right) showing the expression levels of UCP1 (uncoupling protein 1), HIF-1 $\alpha$  (hypoxia-inducible factor-1 $\alpha$ ), and IL-1 $\beta$  (interleukin-1 $\beta$ ) in perivascular adipose tissue (PVAT) of normal chow (NC)- (Group 1), low inorganic phosphate (Pi) hypercaloric (HC)-fed (Group 2), Pi reinstatement (Group 5), and low-Pi NC-fed rats (Group 6). The blots shown are representatives of experiments on tissues from 3 different sets of rats. **B**, Representative micrographs (left) and summary of the quantified data (right) showing the adipocyte size in hematoxylin and eosin (H&E)-stained PVAT sections. Scale bars are 25  $\mu$ m. **C**, Representative micrographs of histopathological, immunohistochemical, and dihydroethidium (DHE) staining in heart midsection. Scale bars are (top to bottom): 25, 25, 50, and 50  $\mu$ m. Fibrotic staining appears as a blue color on a red background, CD68 staining appears as a brown color on a background of H&E counter stain, whereas DHE staining appears as red fluorescence on a black background. Quantification values of area of interfibrillar edema (top left), as well as the intensity of Masson trichrome (top right), CD68 (bottom left), and DHE (bottom right) staining normalized to ventricular tissue area are shown. **D**, Representative micrographs of histopathological and DHE staining in aortas. Scale bars are (top to bottom): 50, 25, and 50  $\mu$ m. Fibrotic staining appears as a blue color on a red background, whereas DHE staining appears as red fluorescence on a background of green collagen autofluorescence. Quantification values of medial thickness (top right), as well as the intensity of Masson trichrome (top left) and DHE (bottom) staining normalized to aortic tissue area are shown. Summary data for micrographs are obtained from 9 sections from 3 different rats per group. Results shown are mean  $\pm$  SEM. Statistical significance was tested by 1-way ANOVA followed by Tukey multiple comparisons test. \*Denotes a *P*-value <0.05 vs NC-fed rat values. DHE indicates dihydroethidium stain; GAPDH, glyceraldehyde-3-phosphate dehydrogenase; H & E, hematoxylin and eosin; HC, hypercaloric chow; HIF-1 $\alpha$ , Hypoxia inducible factor-1 $\alpha$ ; IL-1 $\beta$ , Interleukin 1 $\beta$ ; MT, Masson's trichrome stain; NC, normal chow; and UCP1, Uncoupling protein 1.

not been forthcoming.<sup>17,66–68</sup> Here, we propose dietary phosphate supplementation as a simple approach to mitigate PVAT inflammation and reduce the associated cardiovascular consequences. Not only did prolonged Pi supplementation of a hypercaloric Western diet reduce signs of PVAT inflammation, cardiac autonomic, and cerebrovascular dysfunction, in addition to molecular and histopathological indicators of damage in the heart, blood vessels, and brainstem, a 2-week treatment period had similar outcomes as well.

Typically, Western diets known to induce cardiovascular impairment in humans and animal models

are rich in refined sugars and saturated fat.<sup>69</sup> Such dietary shifts are associated with loss of micronutrients including Pi.<sup>26</sup> The rat model used in the present study received a limited increase in daily caloric intake from saturated fats and refined sugars for 12 weeks, producing a nonobese, hyperinsulinemic prediabetic state.<sup>13,14,34,35,70</sup> This modification was associated with almost a 50% reduction in dietary Pi. In the present study, the salient features of this model were confirmed in the cohort of rats fed a hypercaloric diet with 0.375 mg/kcal Pi, particularly hyperinsulinemia and an increased fat:lean ratio indicative of adipose tissue

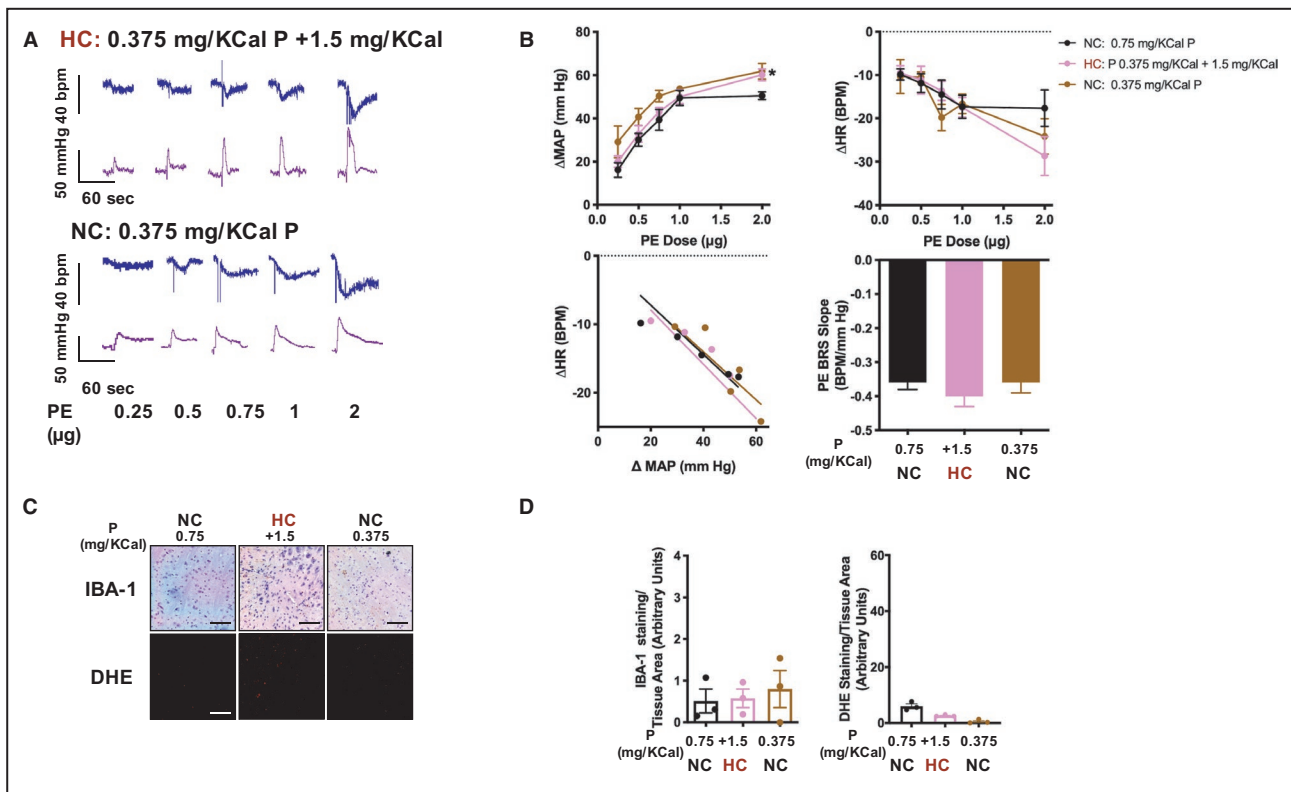


**Figure 8.** Impact of low phosphorus (P) control diet feeding or P reinstatement after a 10-week, high-calorie, phosphorus-deficient diet feeding on parasympathetic cardiac autonomic function and brainstem inflammation.

**A**, Representative tracings of pressor (mean arterial pressure [MAP]) and cardiac (heart rate [HR]) responses to increasing phenylephrine (PE) doses in inorganic phosphate (Pi) reinstatement (Group 5) and low-Pi normal chow (NC)-fed rats (Group 6). Vertical scale bars represent MAP (50 mm Hg) and HR (40 BPM), whereas horizontal scale bars represent time (60 seconds). **B**, The pressor responses to increasing doses of PE (top left), reflex bradycardic responses to increasing blood pressure (top right), best fit regression line for the correlation between  $\Delta$ MAP and reflex changes in HR in response to increasing doses of PE (bottom left), and slope of the linear regression of the relationship between  $\Delta$ HR and  $\Delta$ MAP reflecting parasympathetic baroreceptor sensitivity (BRS; bottom right) Depicted data represent mean $\pm$ SEM of values obtained from 6 rats per group. **C**, Representative micrographs of IBA-1 immunohistochemical and dihydroethidium (DHE) staining in brainstems of low-Pi NC-fed and Pi-reinstatement rats. Data presented are serial sections taken from the same tissues and are representative of 9 sections from 3 different rats in each group. Scale bars are 100  $\mu$ m. IBA-1 staining appears as a brown color on a background of hematoxylin and eosin counter stain, whereas DHE staining appears as red fluorescence on a black background. **D**, Quantification values of IBA-1 staining (left), as well as the intensity of DHE staining (right) normalized to brainstem tissue area are shown. Statistical analysis was done by 2-way ANOVA with repeated measures in the dose factor followed by Sidak multiple comparisons test for  $\Delta$ MAP and  $\Delta$ HR, and 1-way ANOVA followed by Tukey multiple comparisons test for the BRS slope and quantification values in €. \*denotes  $P < 0.05$  vs NC. BRS indicates baroreceptor sensitivity; DHE, dihydroethidium stain; HC, hypercaloric chow; HR, heart rate; IBA-1, ionized calcium-binding adaptor molecule 1; MAP, mean arterial pressure; NC, normal chow; and PE, phenylephrine.

expansion and potential inflammation. Significantly, the insulin spike following simple and refined sugar intake triggered increased peripheral Pi uptake in a manner independent of the status of insulin resistance, further reducing its availability.<sup>71</sup> Moreover, fructose intake, in particular, was shown to reduce serum and intracellular phosphate levels.<sup>72</sup>

Importantly, a considerable body of research demonstrated the beneficial metabolic impact of Pi. Prior findings from our group showed that Pi supplementation reduced postprandial blood glucose and insulin levels,<sup>29</sup> and decreased body weight, body mass index, and waist circumference,<sup>73</sup> increased

postprandial energy expenditure,<sup>74</sup> and preserved the exercise-induced elevation in total energy expenditure potentially by inhibition of energy compensation.<sup>75</sup> Furthermore, other investigators showed that, besides reducing blood glucose, insulin, and lipid levels, phosphate supplementation reduced body fat accumulation, especially in visceral adipose.<sup>76,77</sup>

In this context, increased adipose tissue UCP1 expression was consistently reported in different animals models fed a high-fat diet.<sup>78</sup> Of relevance, UCP1 activity is stimulated by long chain fatty acids increasing in abundance following this kind of diet.<sup>79</sup> UCP1-mediated uncoupling was suggested to be an energy wasting

mechanism to allow sufficient protein intake, especially that this effect was simulated with a diet containing low-quality protein in comparison with another diet containing the phosphate-rich casein.<sup>80</sup> Significantly, although our rat model lacked systemic inflammation,<sup>13,14,35</sup> these rats had localized PVAT inflammation that coincided with increased UCP1 expression and adipocyte hypertrophy resulting in increased hypoxia and inflammation, which were not seen in WAT.<sup>14</sup> In the present study, the same results were recapitulated in the hypercaloric: 0.375 Pi diet. No increases in UCP1 or HIF-1 $\alpha$  expression or in proinflammatory IL-1 $\beta$  level were seen in representative visceral WAT or BAT depots, despite an increase in adipocyte size. This observation confirms the previous suggestion that the growing oxygen demand because of increased UCP1 expression<sup>21–23</sup> possibly underlies the selective vulnerability of PVAT to hypoxia and inflammation at this early stage. Furthermore, the lack of detectable changes in serum levels of leptin and adiponectin, despite an increased fat:lean ratio, supports the notion that the functional and structural deterioration observed in this rat model result from a local paracrine effect of PVAT inflammation rather than a remote effect because of wider involvement of other adipose depots similar to that observed in late stages of obesity and diabetes.<sup>35</sup>

Pi supplementation in rats fed a hypercaloric diet, particularly at the 1.5 mg/kcal dose, reduced serum insulin and lipid levels, as well as adipocyte size. This occurred with a parallel reduction in PVAT UCP1 and HIF-1 $\alpha$  expression levels with a consequent decrease in IL-1 $\beta$ . The amelioration of the PVAT inflammatory status was also demonstrated by a restoration of the macrophage polarization state observed in control rats. Although Pi supplementation did not result in statistically significant changes in calorie intake, body weight, or overall adiposity as measured by fat:lean ratio, a significant restoration of metabolic efficiency was achieved in rats receiving Pi supplementation in a hypercaloric diet. The reduction of metabolic efficiency seen in rats fed hypercaloric: 0.375 could be attributed to increased mitochondrial uncoupling resulting from increased UCP1 expression, hence the dissipation of excess dietary energy as heat. Increased UCP1 expression and activity was shown to be recruited in adipose tissue for diet-induced thermogenesis and was associated with increased oxygen consumption.<sup>81</sup> As such, the restoration of metabolic efficiency in Pi-supplemented rats might be accounted for by the reduction in UCP1 expression and activity. In this regard, the ability of Pi to reduce mitochondrial uncoupling and energy dissipation via the inhibition of UCP1 has been recently shown.<sup>25</sup> Whereas Pi-mediated changes in calorie intake and body weight were below the threshold of statistical significance, the intra-animal normalization involved in the calculation of metabolic

efficiency for each rat in different groups might have accentuated these differences, which are inherently limited given the relatively small size of PVAT being the depot where UCP1 expression is upregulated.

Importantly, although previous studies suggested that Pi supplementation induced a preferential increase in lipid use as an energy source evident by a reduced respiratory quotient without a decrease in oxygen consumption,<sup>77</sup> this appeared to be mediated via coupled mitochondrial respiration. Low serum Pi levels were shown to reduce mitochondrial ATP production,<sup>82</sup> whereas extramitochondrial Pi was shown to induce a balanced activation of the electron transport chain enhancing mitochondrial coupling and ATP production.<sup>83</sup> As such, given the known difference in rates of mitochondrial oxygen consumption between coupled and uncoupled mitochondrial respiration,<sup>84</sup> it becomes plausible that the Pi-induced shift either through inhibition of UCP1, activation of coupled electron transport, or both, underlies the observed alleviation of PVAT hypoxia and inflammation. The increased efficiency of respiration relieving the metabolic stress triggering energy dissipation could explain the observed normalization of UCP1 expression in PVAT from animals receiving phosphate supplementation.

As for the triglyceride levels, although increased serum levels could be tied to increased calorie intake, adipose tissue inflammation was shown to contribute to increased triglyceride levels by a variety of mechanisms including increased insulin resistance.<sup>85</sup> As such, it might be plausible that Pi supplementation could normalize serum triglyceride levels through the amelioration of PVAT inflammation and normalization of insulin levels. A lowering effect on serum lipids was observed for Pi supplementation before.<sup>76,77</sup> However, a potential caveat for this explanation would be the relatively limited impact of a small adipose depot like PVAT on systemic levels of triglycerides. As such, it might be necessary to invoke additional explanations including the overall improvement of metabolism and energy expenditure previously reported for Pi supplementation.

Interestingly, the observed changes occurred in the absence of a detectable alteration of serum phosphate levels. Nevertheless, most authors agree that intracellular phosphate concentration is 3 orders of magnitude higher than that in the extracellular fluid,<sup>86</sup> and particularly, intracellular free phosphate concentration is believed to be 10-fold higher<sup>87</sup>; thus, changes in serum concentration might not be the best reflection of the effect on intracellular targets. However, the results of the in vivo treatment experiments are insufficient to support a direct effect of Pi on PVAT inflammation, particularly that Pi interferes with the function of many pathways with impact on endocrine function and inflammation. In this context, increased Pi intake was found to impact calcium homeostasis and decrease serum calcium



by affecting parathyroid hormone (PTH) levels<sup>88</sup>; however, this has been reported when high Pi intake levels were coupled with reduced calcium intake.<sup>89</sup> Similarly, serum Pi alterations could affect magnesium levels either through renal excretion or via PTH activation.<sup>90</sup> Not only had PTH been implicated in a cross-talk with IL-1 $\beta$  for bone resorption and metabolism,<sup>91</sup> PTH was shown to induce inflammatory IL-6 (interleukin-6) expression in osteoblastic cells.<sup>92</sup> However, in the present study, we did not detect changes in serum calcium or magnesium levels. Furthermore, in a recent study we observed no effect for the range of dietary phosphate supplementation used here on rat serum PTH.<sup>93</sup> As such, the full spectrum of mediators facilitating the effect of phosphate supplementation in vivo remains elusive.

On the other hand, the results of the in vitro cell culture experiments support a direct role of Pi supplementation on PVAT inflammation. Whereas HIF-1 $\alpha$  and IL-1 $\beta$  expression levels increased in the stressed adipocytes exposed to monocytes as observed in the PVAT of prediabetic rats receiving hypercaloric: 0.375, such increases were attenuated in adipocytes exposed to a parallel increase in Pi concentration presumably because of a mitigation of UCP1-mediated oxygen consumption. Nevertheless, it is noteworthy that direct exposure to Pi increased HIF-1 $\alpha$  expression in other cell types including vascular smooth muscle cells.<sup>94</sup> The observed difference could be related to the cell type used; however, the effect of Pi per se on adipocytes in isolation of other factors remains to be determined. As well, direct Pi actions might not only be relevant to the proposed effect on hypoxia. Interestingly, recent investigation proposed CaSR (calcium-sensing receptor) as a mediator of adipose tissue dysfunction, whereby the activation of this receptor was associated with proinflammatory cytokine production.<sup>95,96</sup> On the other hand, other studies showed that selective CaSR knockout in visceral adipose tissue did not alter adipose inflammation and vascular dysfunction induced by a high-fat diet, arguing against its role in this context.<sup>97</sup> Significantly, emerging data suggested that increasing Pi concentration appeared to inhibit CaSR activity by noncompetitive antagonism.<sup>98</sup> However, no appreciable inhibition of CaSR was observed at physiological serum levels of Pi; rather, a 2.5-fold increase was required to achieve this inhibitory effect. As such, the contribution of this mechanism in the context of our present findings showing no increase in serum phosphate remains unlikely.

Under such circumstances, rats receiving a Pi-supplemented hypercaloric diet showed mitigated cardiovascular consequences of PVAT inflammation. As observed previously, hypercaloric: 0.375 Pi feeding was associated with increased vascular reactivity, decreased rate of ventricular contractility, and blunted

parasympathetic baroreflex sensitivity, which were tied to increased paracrine IL-1 $\beta$  production from the inflamed PVAT.<sup>13,14</sup> Pi supplementation, particularly at the 1.5 mg/kcal dose, ameliorated the observed cardiovascular and parasympathetic functional impairment. Moreover, heart midsection and aortic tissue from rats receiving a Pi-supplemented hypercaloric diet showed reduced signs of focal ischemia and decreased medial thickness upon hematoxylin and eosin staining, respectively. As well, fibrosis and oxidative stress were also decreased. Furthermore, our previous work showed that the prediabetic state induced in these rats by hypercaloric feeding increased cerebrovascular tone, triggering an increase in brain oxidative stress and neuroinflammation.<sup>34</sup> Pi supplementation normalized cerebrovascular tone in response to a range of intravascular pressure values and reduced signs of brainstem neuroinflammation and oxidative stress. Cardiac autonomic neuropathy is a major cardiovascular risk factor in prediabetes and is known to emerge from a disproportionate sympathetic activation attributable to hyperinsulinemia.<sup>99</sup> However, it could also be argued that the observed autonomic insult is a consequence of increased brainstem oxidative stress and inflammation.<sup>100</sup> In either case, Pi supplementation appears to reverse hyperinsulinemia and increase cerebrovascular tone, leading to brainstem oxidative stress.

From a different perspective, the ability of Pi administration to improve insulin sensitivity<sup>101</sup> and reduce insulin levels<sup>29</sup> could be invoked to explain the observed effect of Pi supplementation on PVAT. Hyperinsulinemia was proposed as a possible instigator of adipose inflammation via insulin-induced adipocyte hypertrophy.<sup>12</sup> Nevertheless, the insulin-lowering effect of Pi cannot rule out other mechanisms discussed above. This could be inferred from the observations in rats receiving a 2-week treatment protocol of a 1.5 mg/kcal Pi-supplemented diet after being fed an hypercaloric: 0.375 Pi diet for 10 weeks. Whereas the relatively short duration of exposure to Pi supplementation was not sufficient to trigger changes in serum insulin level and adipocyte size, together with a lack of reversal of cumulative metabolic efficiency, this 2-week regimen improved PVAT hypoxia and inflammation, as well as the functional, histological, and molecular manifestations of autonomic and cardiovascular deterioration. These findings suggest that Pi produced a direct insulin-independent PVAT effect, potentially reducing hypoxia by UCP1 inhibition and promoting coupled mitochondrial respiration. On the other hand, Pi deficiency on its own could not explain the observed PVAT and cardiovascular phenotype. A low Pi control diet evoked neither PVAT inflammation nor cardiovascular deterioration, apart from a reduced rate of ventricular contraction. Such a finding is expected, because a diet with standard composition would not be anticipated

to upregulate UCP1. Alternatively, the present findings propose that the decreased phosphate intake might have left oxygen consumption by the increased PVAT UCP1 unopposed and thus augmented hypoxia, HIF-1 $\alpha$  expression, and inflammation.

Despite the availability of information describing the molecular mechanism of Pi in this context and the favorable outcomes of Pi supplementation in early metabolic dysfunction, its recommendation for clinical investigation will be hampered by the perceived adverse effects. Literature shows a biphasic relationship for the impact of serum phosphate level. Whereas lower serum phosphate levels correlated with metabolic impairment leading to increased cardiovascular risk, higher levels were also associated with cardiovascular disease.<sup>27</sup> Moreover, fluctuations in serum phosphate concentrations triggered changes in calcium levels as well as those of the PTH.<sup>101</sup> Importantly, studies showed that high serum phosphate levels or an excessive intake of phosphate were linked to cardiovascular and renal damage.<sup>102,103</sup> In patients with diabetes, in particular, phosphate homeostasis appears to be rather complex and more likely to accelerate renal and cardiovascular complications compared with nondiabetic individuals. For instance, evidence identified serum phosphate as an independent risk factor for the progression of diabetic nephropathy.<sup>104</sup> On the other hand, other evidence implicates hypophosphatemia triggered by decreased phosphate reabsorption in patients with uncontrolled diabetes might contribute to hypoxic damage of retinal and renal tubular cells.<sup>105</sup> Importantly, studies reporting adverse effects of increased Pi intake show clear signs of deposition of calcium phosphate in the kidneys.<sup>89</sup> Increased Pi intake was associated with tubular necrosis and renal calcification in rats, albeit at intake levels that are 3- to 4-fold higher than the highest concentration used in the present study.<sup>61</sup> As well, osteogenic changes including increased runt-related transcription factor 2 (RUNX2) expression and vascular calcification were observed in rats fed a high Pi diet; however, this occurred only in nephrectomized rats receiving more than twice as much Pi as in our highest dietary composition, leading to profound changes in serum Pi and calcium not observed in the present study.<sup>106</sup> Nonetheless, histological examination revealed normal renal glomerular and tubular structure in the kidneys in rats of all groups. Importantly, silver staining showed a total lack of calcium deposits in the kidneys in all groups. Moreover, no differences in serum creatinine levels were observed in any of the treatment groups, possibly indicating normal renal function. Phosphate nephropathy was associated with severely increased serum creatinine that could be detected less than a month from the high phosphate exposure.<sup>107,108</sup> In parallel, histological examination of aortic tissue in our different rat groups did not show

any sign of structural disruption that might be indicative of increased FGF23 (fibroblast growth factor-23) levels induced by increased Pi intake.<sup>109</sup> Interestingly, our recent results showed that FGF23 levels do not change the range of Pi supplementation in rats used in the present study.<sup>93</sup> Moreover, previous research showed that elevated sympathetic activity increased FGF23 production,<sup>110</sup> whereas sympathetic blockade reversed it.<sup>111</sup> Thus, in the high-fat low-phosphate rat group with an autonomic dysfunction favoring sympathetic outflow, FGF23 production might be influenced by 2 opposing physiological stimuli, further attesting to the complexity of the mechanisms at play. Therefore, such a recommendation for Pi intake must be decided within a more holistic process, taking into consideration the overall patient profile, including serum electrolyte, PTH, and insulin levels, as well as kidney function status. This is particularly important because the extrapolation of the present results could not be done directly, because the model used here represents a precise stage in metabolic deterioration with many peculiarities that might not exactly mirror the human metabolic status.

In conclusion, the present study proposes a novel role for Pi supplementation in curbing PVAT inflammation occurring in early metabolic dysfunction triggered by intake of diets with a diluted Pi content. Pi normalization relieves PVAT hypoxia and mitigates the detrimental cardiac autonomic and vascular consequences. The combined metabolic and cardiovascular impact highlights a potential role for Pi in the amelioration of the emergence of the early cardiometabolic complications of increased calorie intake.

## ARTICLE INFORMATION

Received July 18, 2021; accepted October 28, 2021.

### Affiliations

Department of Pharmacology and Toxicology, Faculty of Medicine (H.S.D., G.A., I.A., R.R., N.M., A.F.E.); Department of Nutrition and Food Sciences, Faculty of Agriculture and Food Sciences (H.S.D., M.R., O.O.); and Department of Biochemistry and Molecular Genetics, Faculty of Medicine (I.A., M.R.), The American University of Beirut, Beirut, Lebanon; INSERM UMR 1260, Regenerative Nanomedicine, FMTS, University of Strasbourg, Strasbourg, France (A.M.); Division of Cardiology, Department of Internal Medicine, Faculty of Medicine, The American University of Beirut, Beirut, Lebanon (M.R.); Department of Pharmacology and Toxicology, Faculty of Pharmacy, Alexandria University, Alexandria, Egypt (A.F.E.); and Faculty of Pharmacy, Al-Alamein International University, Alamein, Egypt (A.F.E.).

### Sources of Funding

This work was supported by an American University of Beirut President's Collaborative Research Stimulus Grant to A.F.E., O.O., and M.R. H.S.D. is supported by a Doctoral Scholarship from the Faculty of Agriculture and Food Sciences at the American University of Beirut and a Predoctoral Fellowship from l'Oreal-UNESCO for Women in Science Program.

### Disclosures

None.

### Supplemental Material

Figures S1–S8

## REFERENCES

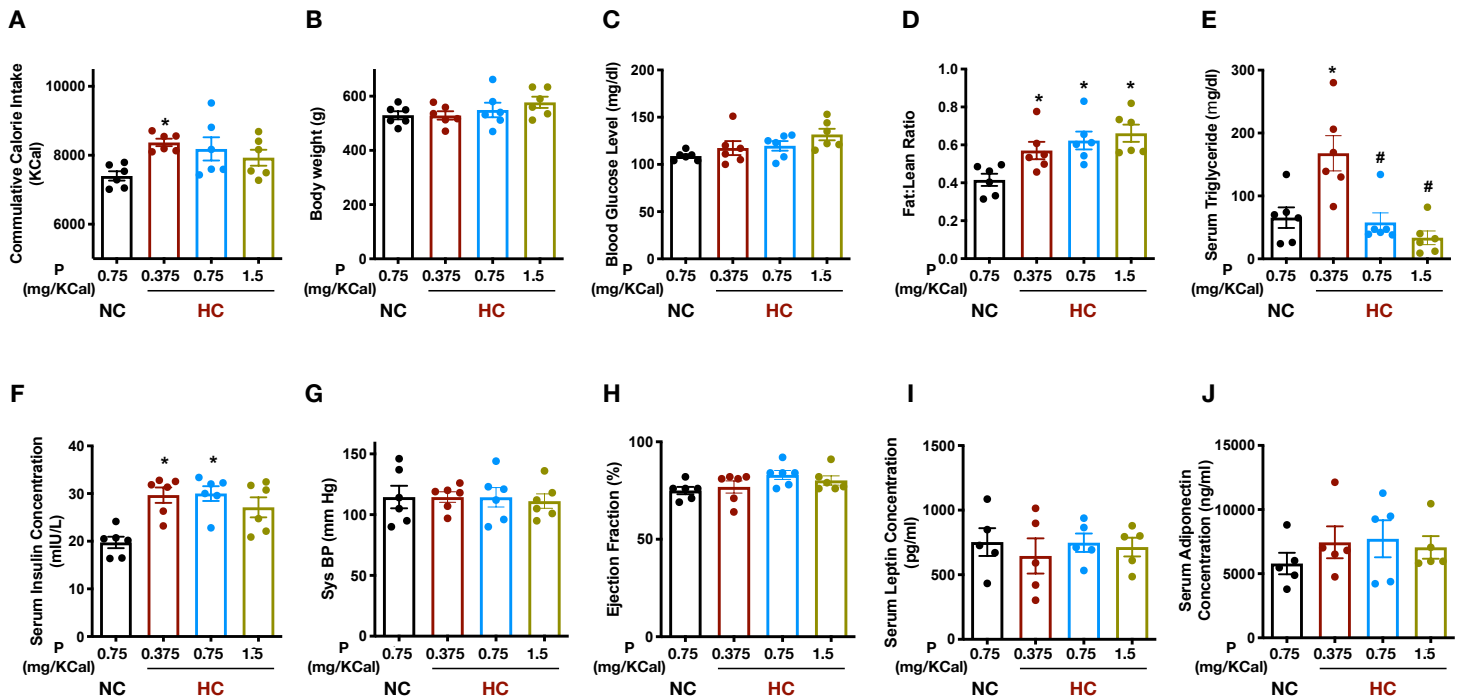
- Malik VS, Willett WC, Hu FB. Global obesity: trends, risk factors and policy implications. *Nat Rev Endocrinol*. 2013;9:13–27. doi: 10.1038/nrendo.2012.199
- Han JC, Lawlor DA, Kimm SYS. Childhood obesity. *Lancet*. 2010;375:1737–1748. doi: 10.1016/S0140-6736(10)60171-7
- Lin X, Xu Y, Pan X, Xu J, Ding Y, Sun X, Song X, Ren Y, Shan P-F. Global, regional, and national burden and trend of diabetes in 195 countries and territories: an analysis from 1990 to 2025. *Sci Rep*. 2020;10:14790. doi: 10.1038/s41598-020-71908-9
- von Bibra H, Paulus W, St. John Sutton M. Cardiometabolic syndrome and increased risk of heart failure. *Curr Heart Fail Rep*. 2016;13:219–229. doi: 10.1007/s11897-016-0298-4
- Ash-Bernal R, Peterson LR. The cardiometabolic syndrome and cardiovascular disease. *J Cardiometab Syndr*. 2006;1:25–28. doi: 10.1111/j.0197-3118.2006.05452.x
- Misra A, Singhal N, Khurana L. Obesity, the metabolic syndrome, and type 2 diabetes in developing countries: role of dietary fats and oils. *J Am Coll Nutr*. 2010;29:289S–301S. doi: 10.1080/07315724.2010.10719844
- Lutsey PL, Steffen LM, Stevens J. Dietary intake and the development of the metabolic syndrome. *Circulation*. 2008;117:754–761. doi: 10.1161/CIRCULATIONAHA.107.716159
- Choe SS, Huh JY, Hwang IJ, Kim JI, Kim JB. Adipose tissue remodeling: its role in energy metabolism and metabolic disorders. *Front Endocrinol*. 2016;7:30. doi: 10.3389/fendo.2016.00030
- Fitzgibbons TP, Czech MP. Epicardial and perivascular adipose tissues and their influence on cardiovascular disease: basic mechanisms and clinical associations. *J Am Heart Assoc*. 2014;3:e000582. doi: 10.1161/JAHA.113.000582
- AlZaim I, Hammoud SH, Al-Koussa H, Ghazi A, Eid AH, El-Yazbi AF. Adipose tissue immunomodulation: a novel therapeutic approach in cardiovascular and metabolic diseases. *Front Cardiovasc Med*. 2020;7:602088. doi: 10.3389/fcvm.2020.602088
- Festa A, Hanley AJ, Tracy RP, D'Agostino R Jr, Haffner SM. Inflammation in the prediabetic state is related to increased insulin resistance rather than decreased insulin secretion. *Circulation*. 2003;108:1822–1830. doi: 10.1161/01.CIR.0000091339.70120.53
- Pedersen DJ, Guilherme A, Danai LV, Heyda L, Matevossian A, Cohen J, Nicoloso SM, Straubhaar J, Noh HL, Jung DY, et al. A major role of insulin in promoting obesity-associated adipose tissue inflammation. *Mol Metab*. 2015;4:507–518. doi: 10.1016/j.molmet.2015.04.003
- Al-Assi O, Ghali R, Mroueh A, Kaplan A, Mougharbil N, Eid AH, Zouein FA, El-Yazbi AF. Cardiac autonomic neuropathy as a result of mild hypercaloric challenge in absence of signs of diabetes: modulation by antidiabetic drugs. *Oxid Med Cell Longev*. 2018;2018:1–19. doi: 10.1155/2018/9389784
- Elkhatib MAW, Mroueh A, Rafeh RW, Sleiman F, Fouad H, Saad EI, Fouda MA, Elgaddar O, Issa K, Eid AH, et al. Amelioration of perivascular adipose inflammation reverses vascular dysfunction in a model of nonobese prediabetic metabolic challenge: potential role of antidiabetic drugs. *Transl Res*. 2019;214:121–143. doi: 10.1016/j.trsl.2019.07.009
- Horimatsu T, Patel AS, Prasad R, Reid LE, Benson TW, Zarzour A, Oghi M, Bruder do Nascimento T, Belin de Chantemele E, Stansfield BK, et al. Remote effects of transplanted perivascular adipose tissue on endothelial function and atherosclerosis. *Cardiovasc Drugs Ther*. 2018;32:503–510. doi: 10.1007/s10557-018-6821-y
- Ahmadieh S, Kim HW, Weintraub NL. Potential role of perivascular adipose tissue in modulating atherosclerosis. *Clin Sci*. 2020;134:3–13. doi: 10.1042/CS20190577
- Rafeh R, Viveiros A, Oudit GY, El-Yazbi AF. Targeting perivascular and epicardial adipose tissue inflammation: therapeutic opportunities for cardiovascular disease. *Clin Sci*. 2020;134:827–851. doi: 10.1042/CS20190227
- Hammoud SH, AlZaim I, Mougharbil N, Koubar S, Eid AH, Eid AA, El-Yazbi AF. Peri-renal adipose inflammation contributes to renal dysfunction in a non-obese prediabetic rat model: role of antidiabetic drugs. *Biochem Pharmacol*. 2021;186:114491. doi: 10.1016/j.bcp.2021.114491
- Hildebrand S, Stümer J, Pfeifer A. PVAT and its relation to brown, beige, and white adipose tissue in development and function. *Front Physiol*. 2018;9:70. doi: 10.3389/fphys.2018.00070
- Szasz T, Webb RC. Perivascular adipose tissue: more than just structural support. *Clin Sci*. 2012;122:1–12. doi: 10.1042/CS20110151
- Shabalina IG, Petrovic N, de Jong JM, Kalinovich AV, Cannon B, Nedergaard J. UCP1 in brite/beige adipose tissue mitochondria is functionally thermogenic. *Cell Rep*. 2013;5:1196–1203. doi: 10.1016/j.celrep.2013.10.044
- Vijgen GHEJ, Sparks LM, Bouvy ND, Schaart G, Hoeks J, van Marken Lichtenbelt WD, Schrauwen P. Increased oxygen consumption in human adipose tissue from the “brown adipose tissue” region. *J Clin Endocrinol Metab*. 2013;98:E1230–E1234. doi: 10.1210/jc.2013-1348
- Schneider K, Valdez J, Nguyen J, Vawter M, Galke B, Kurtz TW, Chan JY. Increased energy expenditure, Ucp1 expression, and resistance to diet-induced obesity in mice lacking nuclear factor-erythroid-2-related transcription factor-2 (Nrf2). *J Biol Chem*. 2016;291:7754–7766. doi: 10.1074/jbc.M115.673756
- Dwaib HS, AlZaim I, Eid AH, Obeid O, El-Yazbi AF. Modulatory effect of intermittent fasting on adipose tissue inflammation: amelioration of cardiovascular dysfunction in early metabolic impairment. *Front Pharmacol*. 2021;12. doi: 10.3389/fphar.2021.626313
- Macher G, Koehler M, Rupprecht A, Kreiter J, Hinterdorfer P, Pohl EE. Inhibition of mitochondrial UCP1 and UCP3 by purine nucleotides and phosphate. *Biochim Biophys Acta*. 2018;1860:664–672. doi: 10.1016/j.bbame.2017.12.001
- Gibson SA. Dietary sugars intake and micronutrient adequacy: a systematic review of the evidence. *Nutr Res Rev*. 2007;20:121–131. doi: 10.1017/S0954422407797846
- Park W, Kim BS, Lee JE, Huh JK, Kim BJ, Sung KC, Kang JH, Lee MH, Park JR, Rhee EJ, et al. Serum phosphate levels and the risk of cardiovascular disease and metabolic syndrome: a double-edged sword. *Diabetes Res Clin Pract*. 2009;83:119–125. doi: 10.1016/j.diabres.2008.08.018
- Hazim J, Hlais S, Ghattas H, Shatila D, Bassil M, Obeid O. Phosphorus supplement alters postprandial lipemia of healthy male subjects: a pilot cross-over trial. *Lipids Health Dis*. 2014;13:109. doi: 10.1186/1476-511X-13-109
- Khatab M, Abi-Rashed C, Ghattas H, Hlais S, Obeid O. Phosphorus ingestion improves oral glucose tolerance of healthy male subjects: a cross-over experiment. *Nutr J*. 2015;14:112. doi: 10.1186/s12937-015-0101-5
- Bassil MS, Obeid OA. Phosphorus supplementation recovers the blunted diet-induced thermogenesis of overweight and obese adults: a pilot study. *Nutrients*. 2016;8:801. doi: 10.3390/nu8120801
- Gutiérrez OM. The connection between dietary phosphorus, cardiovascular disease, and mortality: Where we stand and what we need to know. *Adv Nutr*. 2013;4:723–729. doi: 10.3945/an.113.004812
- National Research Council Committee for the Update of the Guide for the C, Use of Laboratory A. The national academies collection: Reports funded by national institutes of health. In: Garnett N, ed. *Guide for the Care and Use of Laboratory Animals*. Washington (DC): National Academies Press (US) National Academy of Sciences; 2011.
- Reeves PG, Nielsen FH, Fahey GC Jr. AIN-93 Purified diets for laboratory rodents: final report of the American Institute of Nutrition ad hoc writing committee on the reformulation of the AIN-76A rodent diet. *J Nutr*. 1993;123:1939–1951. doi: 10.1093/jn/123.11.1939
- Fakih W, Mroueh A, Salah H, Eid AH, Obeid M, Kobeissy F, Darwish H, El-Yazbi AF. Dysfunctional cerebrovascular tone contributes to cognitive impairment in a non-obese rat model of prediabetic challenge: role of suppression of autophagy and modulation by anti-diabetic drugs. *Biochem Pharmacol*. 2020;178:114041. doi: 10.1016/j.bcp.2020.114041
- Bakkar NZ, Mougharbil N, Mroueh A, Kaplan A, Eid AH, Fares S, Zouein FA, El-Yazbi AF. Worsening baroreflex sensitivity on progression to type 2 diabetes: localized vs. systemic inflammation and role of antidiabetic therapy. *Am J Physiol. Endocrinol Metab*. 2020;319:E835–E851. doi: 10.1152/ajpendo.00145.2020
- Elliott SS, Keim NL, Stern JS, Teff K, Havel PJ. Fructose, weight gain, and the insulin resistance syndrome. *Am J Clin Nutr*. 2002;76:911–922. doi: 10.1093/ajcn/76.5.911
- Dornas WC, de Lima WG, Pedrosa ML, Silva ME. Health implications of high-fructose intake and current research. *Adv Nutr*. 2015;6:729–737.
- Poudyal H, Lemonakis N, Efentakis P, Gikas E, Halabalaki M, Andreadou I, Skaltsounis L, Brown L. Hydroxytyrosol ameliorates metabolic, cardiovascular and liver changes in a rat model of diet-induced metabolic syndrome: pharmacological and metabolism-based investigation. *Pharmacol Res*. 2017;117:32–45. doi: 10.1016/j.phrs.2016.12.002

39. Balakumar M, Raji L, Prabhu D, Sathishkumar C, Prabu P, Mohan V, Balasubramanyam M. High-fructose diet is as detrimental as high-fat diet in the induction of insulin resistance and diabetes mediated by hepatic/pancreatic endoplasmic reticulum (ER) stress. *Mol Cell Biochem*. 2016;423:93–104. doi: 10.1007/s11010-016-2828-5
40. Hazarika A, Kalita H, Chandra Boruah D, Chandra Kalita M, Devi R. Pathophysiology of metabolic syndrome: the onset of natural recovery on withdrawal of a high-carbohydrate, high-fat diet. *Nutrition*. 2016;1081–1091.
41. Peredo HA, Lee H, Donoso AS, Andrade V, Sanchez Eluchans N, Puyo AM. A high-fat plus fructose diet produces a vascular prostanoid alterations in the rat. *Auton Autacoid Pharmacol*. 2015;34:35–40. doi: 10.1111/aap.12021
42. Toklu HZ, Muller-Delp J, Sakaraya Y, Oktay S, Kirichenko N, Matheny M, Carter CS, Morgan D, Strehler KY, Tumer N, et al. High dietary fructose does not exacerbate the detrimental consequences of high fat diet on basilar artery function. *J Physiol Pharmacol : An Official J Polish Physiol Soc*. 2016;67:205–216.
43. Lozano I, Van der Werf R, Bietiger W, Seyfritz E, Peronet C, Pinget M, Jeandier N, Maillard E, Marchioni E, Sigrüst S, et al. High-fructose and high-fat diet-induced disorders in rats: impact on diabetes risk, hepatic and vascular complications. *Nutr Metabol*. 2016;13. doi: 10.1186/s12986-016-0074-1
44. Huang JP, Cheng ML, Hung CY, Wang CH, Hsieh PS, Shiao MS, Chen JK, Li DE, Hung LM. Docosapentaenoic acid and docosahexaenoic acid positively associate with insulin sensitivity in rats fed high-fat and high-fructose diets. *J Diab*. 2017;9:936–946.
45. Huang JP, Cheng ML, Wang CH, Shiao MS, Chen JK, Hung LM. High-fructose and high-fat feeding correspondingly lead to the development of lysoPC-associated apoptotic cardiomyopathy and adrenergic signaling-related cardiac hypertrophy. *Int J Cardiol*. 2016;215:65–76. doi: 10.1016/j.ijcard.2016.03.239
46. Al-Assi O, Ghali R, Mroueh A, Kaplan A, Mougharbil N, Eid AH, Zoueini FA, El-Yazbi AF. Cardiac autonomic neuropathy as a result of mild hypercaloric challenge in absence of signs of diabetes: modulation by antidiabetic drugs. *Oxid Med Cell Longev*. 2018;2018:1–19. doi: 10.1155/2018/9389784
47. Wang Y, Thatcher SE, Cassis LA. Measuring blood pressure using a noninvasive tail cuff method in mice. *Methods Mol Biol*. 2017;1614:69–73.
48. El-Gowell HM, Ibrahim KS, El-Yazbi AF, El-Mas MM. Role of NADPHox/Rho-kinase signaling in the cyclosporine-NSAIDs interactions on blood pressure and baroreflexes in female rats. *Life Sci*. 2017;185:15–22. doi: 10.1016/j.lfs.2017.07.019
49. Levin BE, Finnegan MB, Marquet E, Triscari J, Comai K, Sullivan AC. Effects of diet and obesity on brown adipose metabolism. *Am J Physiol*. 1984;246:E418–E425. doi: 10.1152/ajpendo.1984.246.5.E418
50. Zhang F, Hao G, Shao M, Nham K, An YU, Wang Q, Zhu YI, Kusminski CM, Hassan G, Gupta RK, et al. An adipose tissue atlas: an image-guided identification of human-like bat and beige depots in rodents. *Cell Metab*. 2018;27:252–262.e253. doi: 10.1016/j.cmet.2017.12.004
51. Kim YJ, Park T. Genes are differentially expressed in the epididymal fat of rats rendered obese by a high-fat diet. *Nutr Res*. 2008;28:414–422. doi: 10.1016/j.nutres.2008.03.015
52. El-Yazbi AF, Abd-Elrahman KS, Moreno-Dominguez A. PKC-mediated cerebral vasoconstriction: role of myosin light chain phosphorylation versus actin cytoskeleton reorganization. *Biochem Pharmacol*. 2015;95:263–278. doi: 10.1016/j.bcp.2015.04.011
53. Cho KW, Morris DL, Lumeng CN. Flow cytometry analyses of adipose tissue macrophages. *Methods Enzymol*. 2014;537:297–314.
54. Rubio-Navarro A, Guerrero-Hue M, Martín-Fernandez B, Cortegano I, Olivares-Alvaro E, de las Heras N, Alía M, de Andrés B, Gaspar ML, Egido J, et al. Phenotypic characterization of macrophages from rat kidney by flow cytometry. *J vis Exp*. 2016. doi: 10.3791/54599
55. Fishbein MC. Reperfusion injury. *Clin Cardiol*. 1990;13:213–217. doi: 10.1002/clc.4960130312
56. Wong T-Y, Wu C-Y, Martel J, Lin C-W, Hsu F-Y, Ojcius DM, Lin PY, Young JD. Detection and characterization of mineralo-organic nanoparticles in human kidneys. *Sci Rep*. 2015;5:1–13. doi: 10.1038/srep15272
57. Fink T, Zachar V. Adipogenic differentiation of human mesenchymal stem cells. In: Vemuri M, ed. *Mesenchymal Stem Cell Assays and Applications*. Switzerland: Springer; 2011:243–251.
58. El-Yazbi AF, Johnson RP, Walsh EJ, Takeya K, Walsh MP, Cole WC. Pressure-dependent contribution of rho kinase-mediated calcium sensitization in serotonin-evoked vasoconstriction of rat cerebral arteries. *J Physiol*. 2010;588:1747–1762. doi: 10.1113/jphysiol.2010.187146
59. Morris DL, Singer K, Lumeng CN. Adipose tissue macrophages: phenotypic plasticity and diversity in lean and obese states. *Curr Opin Clin Nutr Metab Care*. 2011;14:341–346. doi: 10.1097/MCO.0b013e328347970b
60. Kazak L, Rahbani JF, Samborska B, Lu GZ, Jedrychowski MP, Lajoie M, Zhang S, Ramsay LC, Dou FY, Tenen D, et al. Ablation of adipocyte creatine transport impairs thermogenesis and causes diet-induced obesity. *Nat Metabol*. 2019;1:360–370. doi: 10.1038/s42255-019-0035-x
61. Chang AR, Anderson C. Dietary phosphorus intake and the kidney. *Annu Rev Nutr*. 2017;37:321–346. doi: 10.1146/annurev-nutr-071816-064607
62. Dokken BB. The pathophysiology of cardiovascular disease and diabetes: beyond blood pressure and lipids. *Diab Spect*. 2008;21:160–165. doi: 10.2337/diaspect.21.3.160
63. Zinman B, Wanner C, Lachin JM, Fitchett D, Bluhmki E, Hantel S, Mattheus M, Devins T, Johansen OE, Woerle HJ, et al. Empagliflozin, cardiovascular outcomes, and mortality in type 2 diabetes. *N Engl J Med*. 2015;373:2117–2128. doi: 10.1056/NEJMoa1504720
64. Marso SP, Daniels GH, Brown-Frandsen K, Kristensen P, Mann JFE, Nauck MA, Nissen SE, Pocock S, Poulter NR, Ravn LS, et al. Liraglutide and cardiovascular outcomes in type 2 diabetes. *N Engl J Med*. 2016;375:311–322. doi: 10.1056/NEJMoa1603827
65. Mahaffey KW, Neal B, Perkovic V, de Zeeuw D, Fulcher G, Erondou N, Shaw W, Fabbrini E, Sun T, Li Q, et al. Canagliflozin for primary and secondary prevention of cardiovascular events. *Circulation*. 2018;137:323–334. doi: 10.1161/CIRCULATIONAHA.117.032038
66. Shah A, Mehta N, Reilly MP. Adipose inflammation, insulin resistance, and cardiovascular disease. *JPEN J Parenter Enteral Nutr*. 2008;32:638–644. doi: 10.1177/0148607108325251
67. Wang Z, Nakayama T. Inflammation, a link between obesity and cardiovascular disease. *Mediators Inflamm*. 2010;2010:1–17. doi: 10.1155/2010/535918
68. Christensen RH, von Scholten BJ, Lehrskov LL, Rossing P, Jørgensen PG. Epicardial adipose tissue: an emerging biomarker of cardiovascular complications in type 2 diabetes? *Ther Adv Endocrinol Metab*. 2020;11:2042018820928824. doi: 10.1177/2042018820928824
69. Valensi P. Hypertension, single sugars and fatty acids. *J Hum Hypertens*. 2005;19:S5–S9. doi: 10.1038/sj.jhh.1001954
70. Alaaeddine R, Elkhatib MAW, Mroueh A, Fouad H, Saad EI, El-Sabban ME, Plane F, El-Yazbi AF. Impaired endothelium-dependent hyperpolarization underlies endothelial dysfunction during early metabolic challenge: increased ROS generation and possible interference with NO function. *J Pharmacol Exp Ther*. 2019;371:567–582. doi: 10.1124/jpet.119.262048
71. Nguyen TQ, Maalouf NM, Sakhaee K, Moe OW. Comparison of insulin action on glucose versus potassium uptake in humans. *Clin J Am Soc Nephrol*. 2011;6:1533–1539.
72. Karczmar GS, Kurtz T, Tavares NJ, Weiner MW. Regulation of hepatic inorganic phosphate and ATP in response to fructose loading: an in vivo <sup>31</sup>P-NMR study. *Biochem Biophys Acta*. 1989;1012:121–127. doi: 10.1016/0167-4889(89)90084-0
73. Ayoub JJ, Samra MJ, Hlais SA, Bassil MS, Obeid OA. Effect of phosphorus supplementation on weight gain and waist circumference of overweight/obese adults: a randomized clinical trial. *NutrDiab*. 2015;5:e189. doi: 10.1038/nutd.2015.38
74. Assaad M, El Mallah C, Obeid O. Phosphorus ingestion with a high-carbohydrate meal increased the postprandial energy expenditure of obese and lean individuals. *Nutrition*. 2019;57:59–62. doi: 10.1016/j.nut.2018.05.019
75. Sawaya SW, Ragi ME, Eid AA, Obeid OA. Daily energy expenditure in rats following structured exercise training is affected by dietary phosphorus content. *Br J Nutr*. 2020;126:1110–1120. doi: 10.1017/S0007114520004985
76. Imi Y, Yabiki N, Abuduli M, Masuda M, Yamanaka-Okumura H, Taketani Y. High phosphate diet suppresses lipogenesis in white adipose tissue. *J Clin Biochem Nutr*. 2018;63:181–191. doi: 10.3164/jcbn.17-141
77. Abuduli M, Ohminami H, Otani T, Kubo H, Ueda H, Kawai Y, Masuda M, Yamanaka-Okumura H, Sakae H, Yamamoto H, et al. Effects of dietary phosphate on glucose and lipid metabolism. *Am J Physiol*

- Endocrinol Metabol.* 2016;310:E526–E538. doi: 10.1152/ajpen do.00234.2015
78. Fromme T, Klingenspor M. Uncoupling protein 1 expression and high-fat diets. *Am J Physiol. Regul, Integrative Comp Physiol.* 2011;300:R1–R8. doi: 10.1152/ajpregu.00411.2010
  79. Fedorenko A, Lishko PV, Kirichok Y. Mechanism of fatty-acid-dependent UCP1 uncoupling in brown fat mitochondria. *Cell.* 2012;151:400–413. doi: 10.1016/j.cell.2012.09.010
  80. Torre-Villalvazo I, Tovar AR, Ramos-Barragán VE, Cerbón-Cervantes MA, Torres N. Soy protein ameliorates metabolic abnormalities in liver and adipose tissue of rats fed a high fat diet. *J Nutr.* 2008;138:462–468. doi: 10.1093/jn/138.3.462
  81. Luijten IHN, Feldmann HM, Gv E, Cannon B, Nedergaard J. In the absence of UCP1-mediated diet-induced thermogenesis, obesity is augmented even in the obesity-resistant 129s mouse strain. *Am J Physiol-Endocrinol Metabol.* 2019;316:E729–E740. doi: 10.1152/ajpen do.00020.2019
  82. Pesta DH, Tsirigotis DN, Befroy DE, Caballero D, Jurczak MJ, Rahimi Y, Cline GW, Dufour S, Birkenfeld AL, Rothman DL, et al. Hypophosphatemia promotes lower rates of muscle ATP synthesis. *FASEB J.* 2016;30:3378–3387. doi: 10.1096/fj.201600473R
  83. Bose S, French S, Evans FJ, Joubert F, Balaban RS. Metabolic network control of oxidative phosphorylation: multiple roles of inorganic phosphate. *J Biol Chem.* 2003;278:39155–39165. doi: 10.1074/jbc.M306409200
  84. Ramsay RR. Electron carriers and energy conservation in mitochondrial respiration. *ChemTexts.* 2019;5:9. doi: 10.1007/s40828-019-0085-4
  85. van de Woestijne AP, Monajemi H, Kalkhoven E, Visseren FL. Adipose tissue dysfunction and hypertriglyceridemia: mechanisms and management. *Obes Rev.* 2011;12:829–840. doi: 10.1111/j.1467-789X.2011.00900.x
  86. Yano S, Sugimoto T. Clinical aspect of recent progress in phosphate metabolism. Distribution of phosphorus and its physiological roles in the body: the form, distribution, and physiological function. *Clin Calcium.* 2009;19:771–776.
  87. Cohn SH, Dombrowski CS. Measurement of total-body calcium, sodium, chlorine, nitrogen, and phosphorus in man by in vivo neutron activation analysis. *J Nucl Med.* 1971;12:499–505.
  88. Vorland CJ, Stremke ER, Moorthi RN, Hill Gallant KM. Effects of excessive dietary phosphorus intake on bone health. *Curr Osteoporos Rep.* 2017;15:473–482. doi: 10.1007/s11914-017-0398-4
  89. Katsumata S, Matsuzaki H, Uehara M, Suzuki K. Effects of dietary calcium supplementation on bone metabolism, kidney mineral concentrations, and kidney function in rats fed a high-phosphorus diet. *J Nutr Sci Vitaminol.* 2015;61:195–200. doi: 10.3177/jnsv.61.195
  90. Abbas Raza S, Drezner MK. 33 - phosphorus and magnesium. In: Kleerekoper M, Siris ES, McClung M, eds. *The Bone and Mineral Manual*, 2nd ed. Burlington: Academic Press; 2005:165–172.
  91. Lee Y-M, Fujikado N, Manaka H, Yasuda H, Iwakura Y. Il-1 plays an important role in the bone metabolism under physiological conditions. *Int Immunol.* 2010;22:805–816. doi: 10.1093/intimm/dxq431
  92. Nagy Z, Radeff J, Stern PH. Stimulation of interleukin-6 promoter by parathyroid hormone, tumor necrosis factor  $\alpha$ , and interleukin-1 $\beta$  in UMR-106 osteoblastic cells is inhibited by protein kinase C antagonists. *J Bone Miner Res.* 2001;16:1220–1227. doi: 10.1359/jbmr.2001.16.7.1220
  93. Sawaya SW, Ragi ME, Eid AA, Obeid OA. Daily energy expenditure in rats following structured exercise training is affected by dietary phosphorus content. *Br J Nutr.* 2021;126:1110–1120. doi: 10.1017/S0007114520004985
  94. Mokas S, Larivière R, Lamalice L, Gobeil S, Cornfield DN, Agharazii M, Richard DE. Hypoxia-inducible factor-1 plays a role in phosphate-induced vascular smooth muscle cell calcification. *Kidney Int.* 2016;90:598–609. doi: 10.1016/j.kint.2016.05.020
  95. Bravo-Sagua R, Mattar P, Diaz X, Lavandero S, Cifuentes M. Calcium sensing receptor as a novel mediator of adipose tissue dysfunction: mechanisms and potential clinical implications. *Front Physiol.* 2016;7:395. doi: 10.3389/fphys.2016.00395
  96. Mattar P, Sanhueza S, Yuri G, Briones L, Perez-Leighton C, Rudich A, Lavandero S, Cifuentes M. Calcium-sensing receptor in adipose tissue: possible association with obesity-related elevated autophagy. *Int J Mol Sci.* 2020;21:7617. doi: 10.3390/ijms21207617
  97. Sundaraman SS, Peters LJ, Jansen Y, Gencer S, Yan YI, Nazir S, Bonnin Marquez A, Kahles F, Lehrke M, Biessen EAL, et al. Adipocyte calcium sensing receptor is not involved in visceral adipose tissue inflammation or atherosclerosis development in hyperlipidemic apoE $^{-/-}$  mice. *Sci Rep.* 2021;11:10409. doi: 10.1038/s41598-021-89893-y
  98. Centeno PP, Herberger A, Mun H-C, Tu C, Nemeth EF, Chang W, Conigrave AD, Ward DT. Phosphate acts directly on the calcium-sensing receptor to stimulate parathyroid hormone secretion. *Nat Commun.* 2019;10:4693. doi: 10.1038/s41467-019-12399-9
  99. Bakkar NZ, Dwaib HS, Fares S, Eid AH, Al-Dhaheer Y, El-Yazbi AF. Cardiac autonomic neuropathy: a progressive consequence of chronic low-grade inflammation in type 2 diabetes and related metabolic disorders. *Int J Mol Sci.* 2020;21. doi: 10.3390/ijms21239005
  100. Cruz JC, Flór AFL, França-Silva MS, Balarini CM, Braga VA. Reactive oxygen species in the paraventricular nucleus of the hypothalamus alter sympathetic activity during metabolic syndrome. *Front Physiol.* 2015;6:384. doi: 10.3389/fphys.2015.00384
  101. Nowicki M, Fliser D, Fode P, Ritz E. Changes in plasma phosphate levels influence insulin sensitivity under euglycemic conditions. *J Clin Endocrinol Metabol.* 1996;81:156–159.
  102. Matsuzaki H, Uehara M, Suzuki K, Liu QL, Sato S, Kanke Y, Goto S. High phosphorus diet rapidly induces nephrocalcinosis and proximal tubular injury in rats. *J Nutr Sci Vitaminol (Tokyo).* 1997;43:627–641. doi: 10.3177/jnsv.43.627
  103. Lau WL, Pai A, Moe SM, Giachelli CM. Direct effects of phosphate on vascular cell function. *Adv Chronic Kidney Dis.* 2011;18:105–112. doi: 10.1053/j.ackd.2010.12.002
  104. Xiang H, Zhang H, Zhou M, Jiang S, Zhang L, Chen D, Liu Z. Phosphorus is an independent risk factor for the progression of diabetic nephropathy. *Adv Clin Exp Med.* 2018;27:1239–1245.
  105. Ditzel J, Lervang HH. Disturbance of inorganic phosphate metabolism in diabetes mellitus: its impact on the development of diabetic late complications. *Curr Diabetes Rev.* 2010;6:323–333.
  106. Gracioli FG, Neves KR, dos Reis LM, Gracioli RG, Noronha IL, Moyses RMA, Jorgetti V. Phosphorus overload and PTH induce aortic expression of Runx2 in experimental uraemia. *Nephrol Dial Transplant.* 2008;24:1416–1421. doi: 10.1093/ndt/gfn686
  107. Markowitz GS, Stokes MB, Radhakrishnan J, D'Agati VD. Acute phosphate nephropathy following oral sodium phosphate bowel purgative: an underrecognized cause of chronic renal failure. *J Am Soc Nephrol.* 2005;16:3389–3396. doi: 10.1681/ASN.2005050496
  108. Markowitz GS, Perazella MA. Acute phosphate nephropathy. *Kidney Int.* 2009;76:1027–1034. doi: 10.1038/ki.2009.308
  109. Kuro-o M. The FGF23 and klotho system beyond mineral metabolism. *Clin Exp Nephrol.* 2017;21:64–69. doi: 10.1007/s10157-016-1357-6
  110. Kawai M, Kinoshita S, Shimba S, Ozono K, Michigami T. Sympathetic activation induces skeletal FGF23 expression in a circadian rhythm-dependent manner. *J Biol Chem.* 2014;289:1457–1466. doi: 10.1074/jbc.M113.500850
  111. Fajol A, Chen H, Umbach AT, Quarles LD, Lang F, Föller M. Enhanced FGF23 production in mice expressing PI3K-insensitive GSK3 is normalized by  $\beta$ -blocker treatment. *FASEB J.* 2016;30:994–1001. doi: 10.1096/fj.15-279943

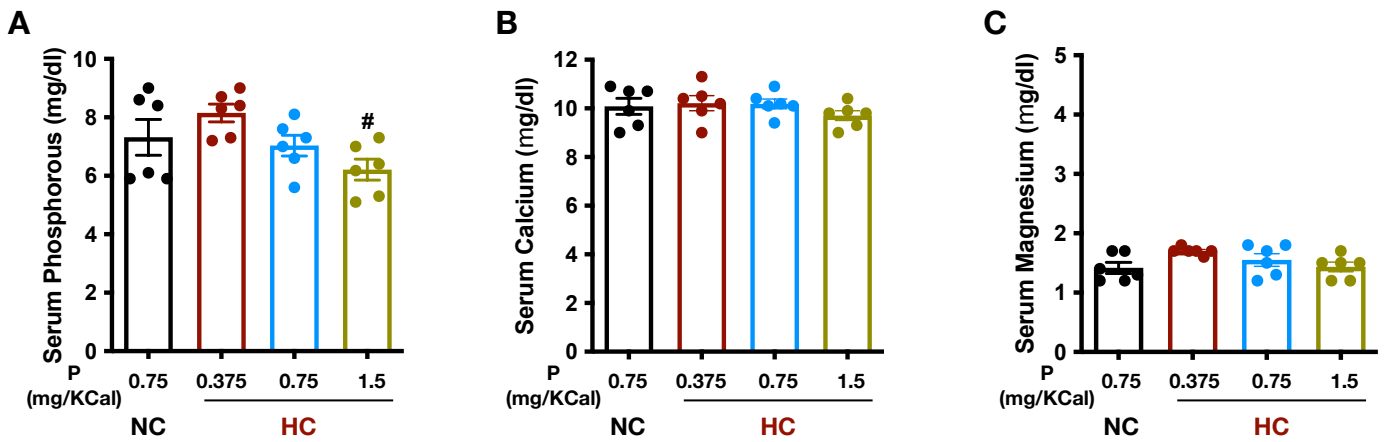
# **SUPPLEMENTAL MATERIAL**

Figure S1



**Figure S1. Metabolic and gross hemodynamic impact of inorganic phosphorus supplementation of hypercaloric diet.** Twelve weeks of increased calorie consumption (A) due to hypercaloric (HC) diet feeding induce a non-obese prediabetic phenotype in rats without an increase in body weight (B), fasting blood glucose (C), systolic blood pressure (Sys BP, G), Ejection fraction (H), Serum Leptin (I), and serum adiponectin (J); but with increased fat:lean ratio (D), serum triglycerides (E), and fasting serum insulin (F). The effects of inorganic phosphorus (P) supplementation at 0.75 and 1.5 mg/Kcal during the full twelve-week duration are depicted and compared to rats receiving normal chow (NC). Results shown are mean  $\pm$  SEM of observations from six different rats per group. Statistical significance was tested by one-way ANOVA followed by Tukey *post hoc* test. \* denotes a *P*-value < 0.05 vs. NC while # denotes a *P*-value < 0.05 vs. HC: 0.375 mg/Kcal P.

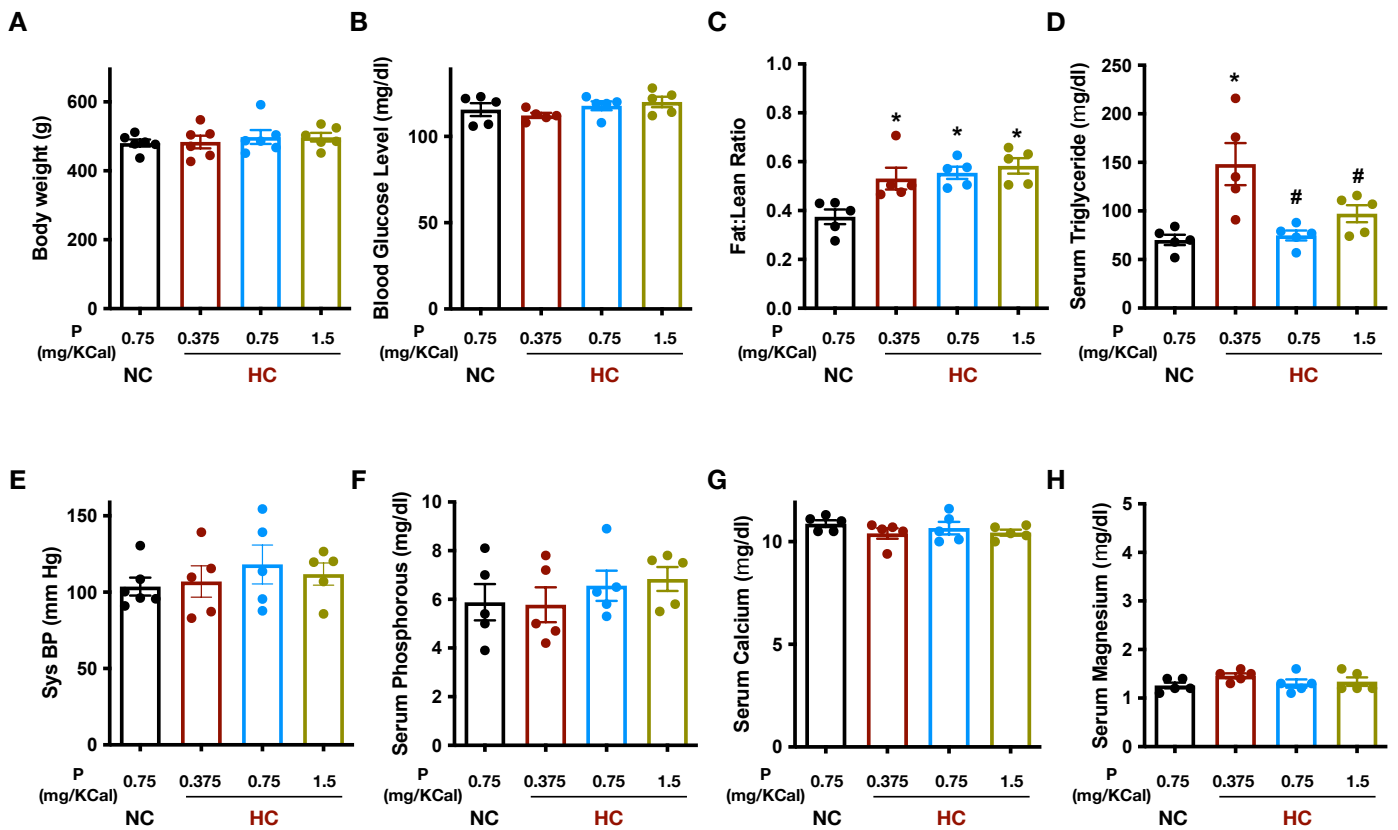
Figure S2



**Figure S2. Phosphorus supplementation does not affect serum Pi, calcium, or magnesium concentrations.** Phosphorus (Pi) deficient hypercaloric feeding (HC: 0.375 mg/Kcal) does not affect serum Pi (A), calcium (B) or magnesium (C) concentrations. Results shown are mean  $\pm$  SEM of observations from six different rats per group. Statistical significance was tested by one-way ANOVA followed by Tukey multiple comparisons test.

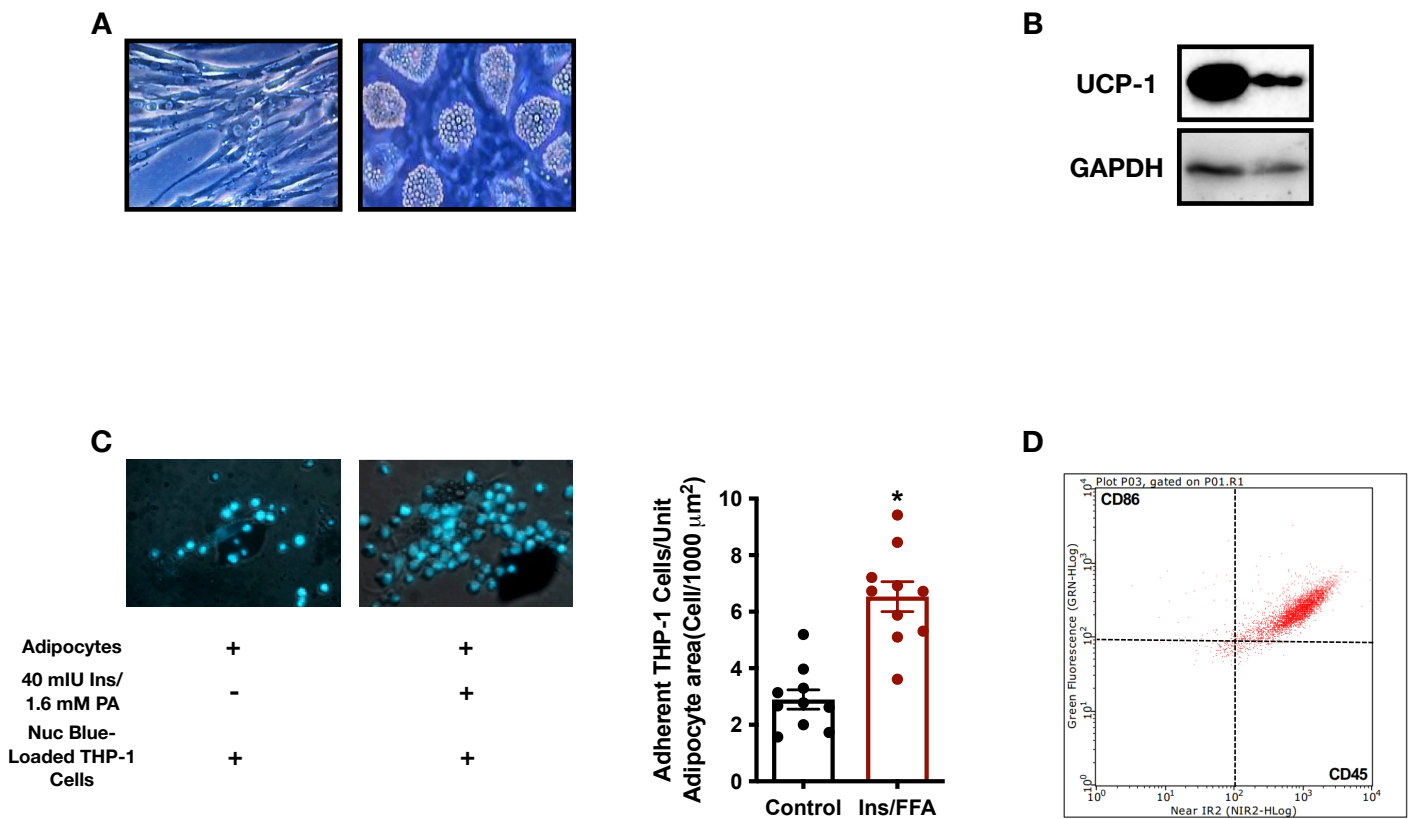


Figure S3



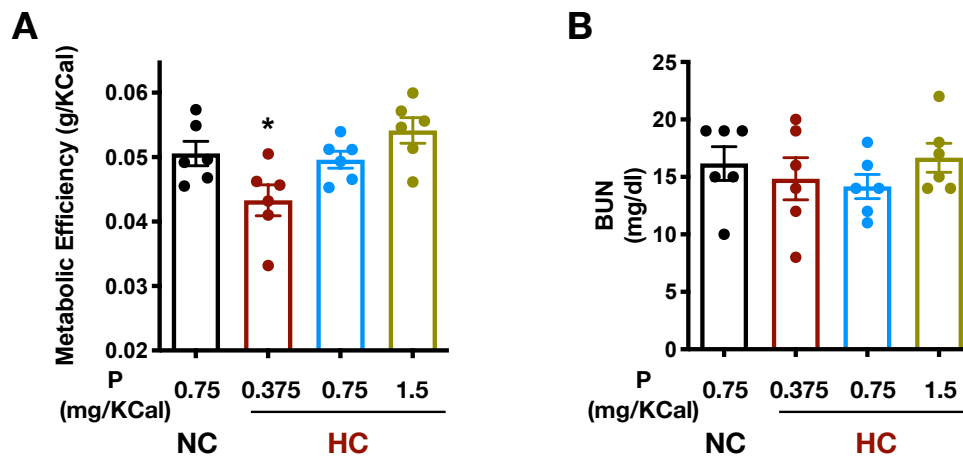
**Figure S 3. Impact of 8 weeks of inorganic phosphorus supplementation of hypercaloric diet on metabolic and gross hemodynamic parameters as well as Pi, calcium, and magnesium concentration.** Eight weeks of feeding had no effect on body weight (A), fasting blood glucose (B), systolic blood pressure (Sys BP, E), serum Pi (F), serum calcium (G), and serum magnesium (H); but increased fat:lean ratio (E) and serum triglycerides (D). Results shown are mean  $\pm$  SEM of observations from five different rats per group. Statistical significance was tested by one-way ANOVA followed by Tukey *post hoc* test. \* denotes a *P*-value < 0.05 vs. NC while # denotes a *P*-value < 0.05 vs. HC: 0.375 mg/Kcal P.

Figure S4



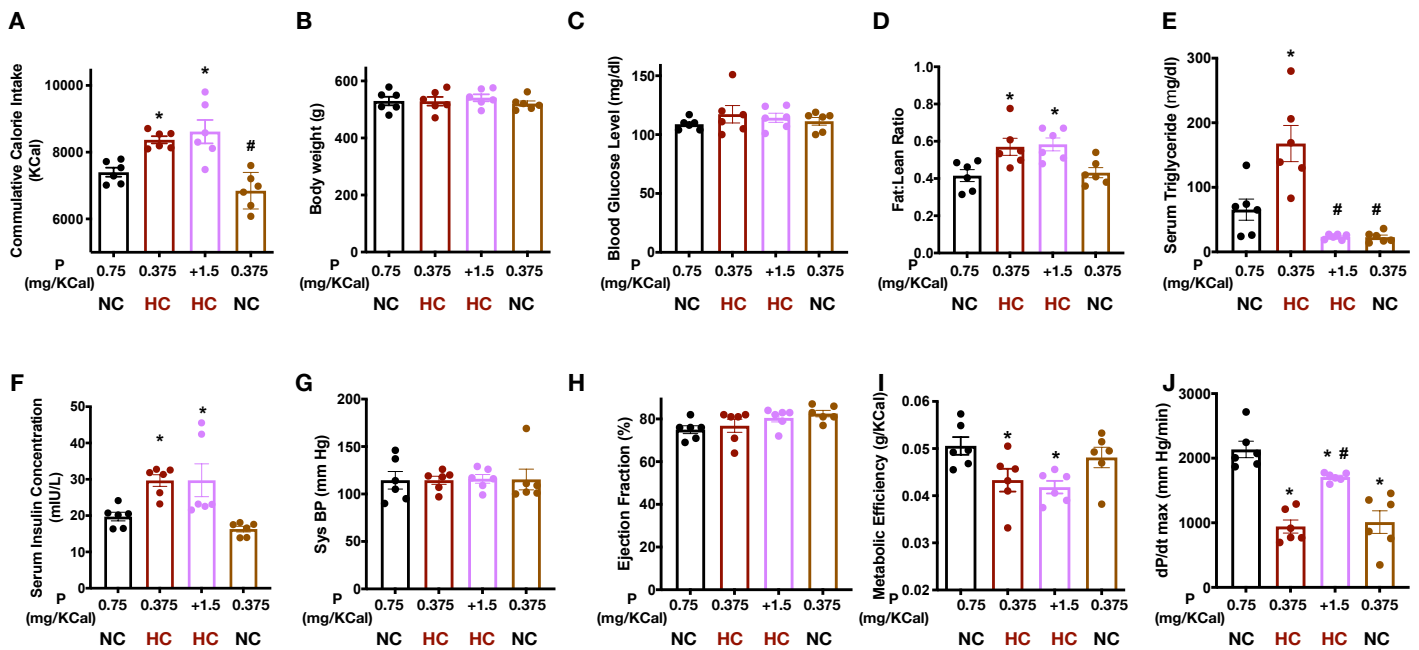
**Supplementary Figure 5. Adipocytes differentiated from human bone marrow-derived mesenchymal stem cells respond to stress by 40 mIU/L insulin and 1.6 mM palmitic acid by an inflamed phenotype.** A, Bone marrow mesenchymal stem cells before (left) and after (right) differentiation to adipocytes; B, Representative western blotting showing UCP1 expression in different batches of differentiated adipocytes; C, adipocyte exposure to a high insulin and palmitic acid stress leads to increased recruitment and adhesion of THP-1 monocytes; D, Recruited monocytes show markers of differentiation into macrophages. For C, statistical significance was tested by *t* test. \* denotes a *P*-value < 0.05 vs. control culture medium without the increased insulin and palmitic acid.

Figure S5



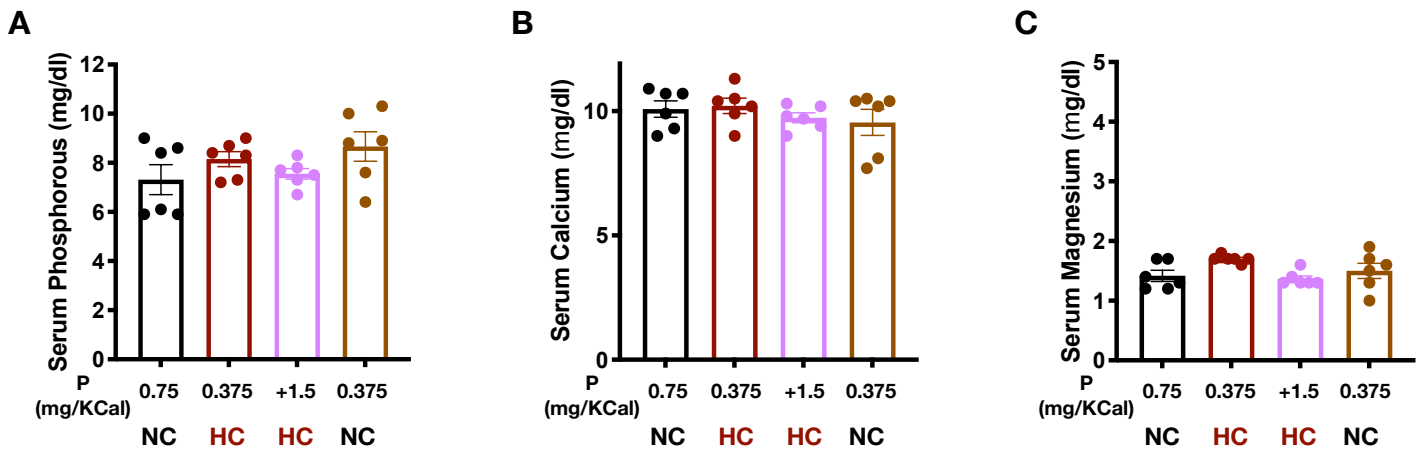
**Figure S 5. Phosphorus supplementation restores metabolic efficiency without affecting protein metabolism.** Phosphorus (Pi) deficient hypercaloric feeding (Group 2: HC: 0.375 mg/Kcal) is associated with reduced metabolic efficiency (A) that is restored by Pi supplementation (Groups 3 & 4) without affecting protein breakdown measured by blood urea nitrogen (BUN, B). Results shown are mean  $\pm$  SEM of observations from six different rats per group. Statistical significance was tested by one-way ANOVA followed by Tukey multiple comparisons test. \* denotes a *P*-value < 0.05 vs. NC-fed rat values.

Figure S6



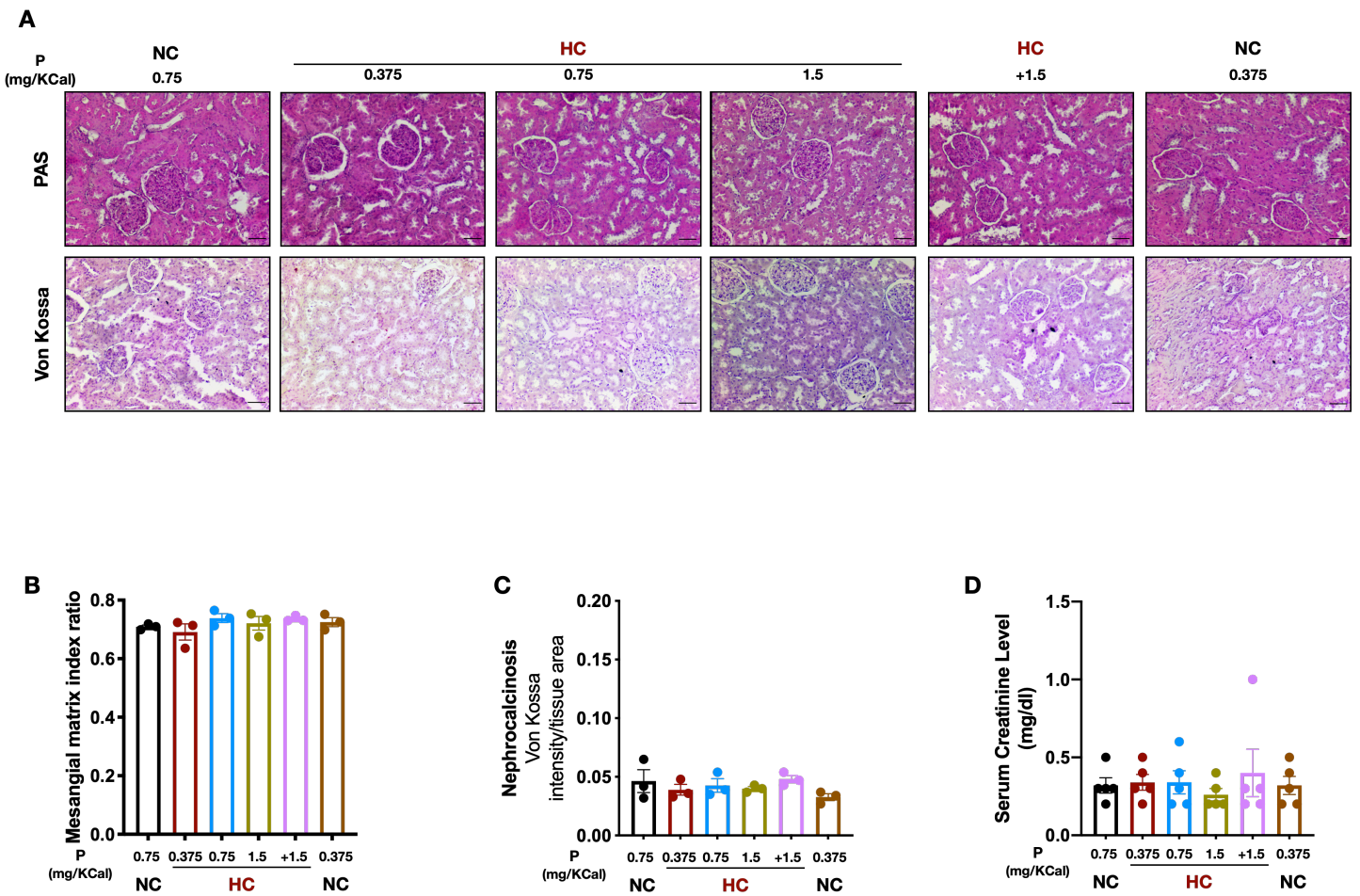
**Figure S6. Gross metabolic and functional parameters following phosphorus reinstatement after a ten-week high calorie phosphorus deficient diet feeding (Group 5) or low phosphorus control diet feeding (Group 6).** The differences in calorie consumption (A) in different groups for the twelve-week duration did not reflect into changes in body weight (B), fasting blood glucose (C), systolic blood pressure (Sys BP, G), and Ejection fraction (H); yet increased fat:lean ratio (D), serum triglycerides (E), and fasting serum insulin (F) were not seen in the low Pi control diet group with only serum triglycerides reversed by Pi reinstatement. Low Pi control diet and Pi reinstatement did not affect metabolic efficiency (I) compared to control rats or those receiving low Pi HC diet, respectively. J, Systolic ventricular function in different groups measured as  $dP/dt_{max}$ . Results shown are mean  $\pm$  SEM of observations from six different rats per group. Statistical significance was tested by one-way ANOVA followed by Tukey *post hoc* test. \* denotes a  $P$ -value  $< 0.05$  vs. NC while # denotes a  $P$ -value  $< 0.05$  vs. HC: 0.375 mg/Kcal P.

Figure S7



**Figure S 7. Serum Pi, calcium and magnesium following phosphorus reinstatement after a ten-week high calorie phosphorus deficient diet feeding (Group 5) or low phosphorus control diet feeding (Group 6).** Different dietary interventions do not affect serum Pi (A), calcium (B) or magnesium (C) concentrations. Results shown are mean  $\pm$  SEM of observations from six different rats per group. Statistical significance was tested by one-way ANOVA followed by Tukey multiple comparisons test.

Figure S8



**Figure S8. Impact of different phosphate and fat levels in diet on renal microscopical structure and calcium deposition, as well as serum creatinine levels.** A, Representative micrographs of PAS (top) and von Kossa (bottom) stained renal cortical sections showing normal glomerular and tubular structure and absence of calcium deposits in kidneys from different treatment groups. Data presented are serial sections taken from the same tissues and are representative of 9 sections from 3 different rats in each group. Scale bars are 50  $\mu$ m. von Kossa staining typically appear as brown staining on a background of H&E counter stain. Quantification values of mesangial matrix ratio reflecting glomerular structure (B), as well as the intensity of von Kossa stain (C), whereas (D) represents average serum creatinine concentration in different treatment groups. Statistical significance was tested by one-way ANOVA followed by Tukey multiple comparisons test.